Bachelor Integration Project IEM

Faculty of Science and Engineering

Stability assessment of a floating hybrid wind-wave platform: a frequency signal analysis

Ocean Grazer

Author

J. Sijtsma | S3342921

Supervisors

prof. dr. A. Vakis

ir. T.M. Kousemaker

June 5, 2020

Abstract

In recent years, there has been an increasing amount of research dedicated to the transition of offshore wind-energy production towards deep water deployment, usually by means of floating platforms. The stability of a floating wind-turbine system is of primary concern. Therefore, this research project has assessed the stability of a floating hybrid wind-wave platform design, which has been conceptualised by Ocean Grazer. By means of the open source Boundary Element Method (BEM) program NEMOH, the static and dynamic response of the structure to regular waves with unitary amplitude have been obtained. It has been shown that the structure is statically stable. Moreover, the dynamic response has been obtained, including resonance frequencies for the motions heave and pitch. In terms of dynamic stability, a fitted transfer function to the pitch frequency data has indicated stability through the location of the poles. Finally, the procedure has been repeated for the structure with a rounded bow shape, in order to compare the surge response to the first case. However, the surge response is similar and therefore the result is indecisive. Further research has been suggested on the round bow shape, the inclusion of the wind effect and mooring and a time-domain analysis.

Contents

List of Figures

List of Tables

List of abbreviations

BEM Boundary Element Method. i, 18, 37, 41

BVPs Boundary Value Problems. 18

CAD Computer Aided Design. 17

DOF Degrees Of Freedom. v, vi, 2, 13–16, 18, 30, 31, 33, 36–38, 42

FHWWP Floating Hybrid Wind-Wave Platform. 5–9, 13–15, 17, 20, 21, 23, 30–35, 37, 41, 42

LHP Left Hand Plane. 17

NSE Navier-Stokes Equations. 11

RAO Response Amplitude Operator. vi, 15, 16, 18, 30, 31, 33, 34, 36, 40–42

RHP Right Hand Plane. 17

SIT System Identification Toolbox. vi, 19, 34, 38, 49–51

WEC Wave Energy Converter. v, 7, 11, 13, 20, 22, 41

Nomenclature

η	Convergence error	-
λ	Wavelength	m
ω	Wave frequency	rad/s
ω_n	Natural frequency	rad/s
ρ_f	Fluid density	kg/m^3
ζ_a	Wave amplitude	m
b	Frequency dependent hydrodynamic damping	Kg/s
c	Phase velocity	m/s
F_B	Buoyancy force	N
F_g	Gravitational force	N
F_{ex}	Frequency dependent excitation force	N
F_{hs}	Hydrostatic restoring force	N
F_{rad}	Radiation force	N
g	Gravitational constant	m/s^2
H	Wave height	m
h	Water depth	m
k	Wave number	rad/m
k_{hs}	Hydrostatic stiffness coefficient	$N/m, Nm/rad$
m	Body mass	Kg
m_a	Frequency dependent added mass	Kg
m_t	Total structure mass	tonnes
$m_{platform}$	Platform mass	tonnes
$m_{turbine}$	Wind-turbine mass	tonnes
T	Wave period	s
V_{disp}	Displaced volume of fluid	m^3
z	Displacement	m, rad

1 Introduction

In the past decade, global primary energy consumption has steadily grown at 2,1% per year (Armaroli and Balzani 2016). Along with an increase of energy usage, Gielen et al. (2019) have reported that in 2015, the total share of renewable energy in total energy generation had been around 25%. However, based on an analysis by IRENA (2019), Gielen et al. (2019) further identified that the share of renewable energy sources should account for roughly 60% in 2030. Therefore, it is evident that renewable energy should undergo a significant expansion in order to decarbonise the energy sector. A company that has invested itself into decarbonising the energy sector is Ocean Grazer B.V, which is a Dutch start-up focusing on developing and commercialising new concepts in order to create a hybrid energy future. In fact, Ocean Grazer is exploring the possibility to implement wind and wave energy generation into a single system. In order to deploy such a hybrid wind-wave system, a floating platform has been conceptualised. However, especially in terms of stability, a floating wind turbine platform faces significant challenges (Liu et al. 2016).

This research project is aimed at assessing the stability of a floating hybrid wind-wave platform, as proven by a computer simulation. Although the project concerns a hybrid platform, the methods and findings might be applicable for other floating structures. By examining the stability of a platform design under the influence of wave induced motions, general applicable knowledge has been generated, which in turn has expanded the current knowledge base.

Firstly, in chapter 2, an overview of background knowledge imperative to the further narrative of this research project has been provided. Secondly, in chapter 3, the problem has been unravelled and the stakeholders, system, problem statement, research objective and research questions have been described. Thereafter, the methodology in terms of theory and applied tools has been provided in chapter 4. In chapter 5, an embodiment of the conceptual design by Ocean Grazer to be used in the analysis has been presented. Consequently, the obtained mesh from the platform embodiment has been tested for convergence in chapter 6, in order to ensure accurate results. Based on the aforementioned chapters, the results of the analysis have been presented in chapter 7, including the hydrostatic and hydrodynamic response and stability assessment of two cases; a square bow shape and rounded bow shape. Furthermore, the validity of the obtained results has been discussed. Consequently, the limitations of the obtained results have been discussed in chapter 8. Finally, each research question introduced in chapter 3 has been considered in order to form a final conclusion.

2 Background knowledge

In order to properly understand the problem definition, it is deemed necessary to describe certain definitions regarding floating objects. Therefore, the sections below describe the different types of motions of floating objects, theory on hydrostatic stability and specifically how stability can be defined.

2.1 Types of motion

The motions of any floating object, such as ships, platforms and buoys, can be described in six Degrees Of Freedom (DOF) (Newman 2018). From the six DOF, three can be classified as translational motions parallel to the three axes of the coordinate system: heave, surge and sway. The remaining three motions are rotational around the same three axes: roll, yaw and pitch. A graphical overview can be seen in Figure 2.1 below. In general, the motion, velocity and acceleration of each of the respective six motions can be defined. In certain situations, specific motions such as sway, roll and yaw may be neglected. Regarding Figure 2.1 below, this is for instance the case when the wave direction is in the negative x_1 direction perpendicular to x_3.

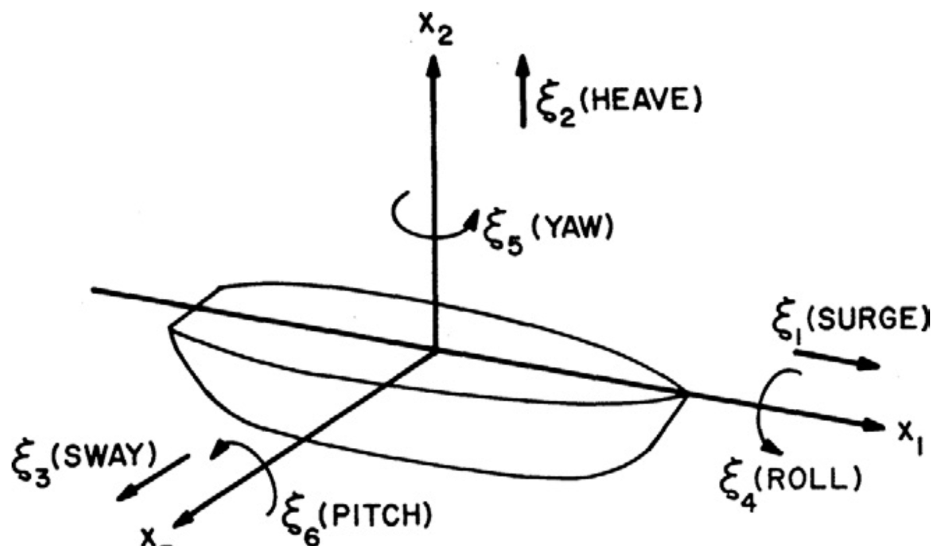

Figure 2.1: Motions in six DOF (Newman 2018)

2.2 Hydrostatic stability

Initially, the stability of a floating structure is determined in a static situation. The main hydrostatic stability criterion is determined by the metacentric height, which is the distance between the centre of gravity G and the metacentre M. The metacentre is obtained from the intersection between the centreline of a floating structure and the line of action of buoyancy. A requirement of stability is then that the metacentre is above the centre of gravity and the metacentric height $GM > 0$ (Thiagarajan and Dagher 2014). A hydrostatic system under a certain angle has schematically been portrayed in Figure 2.2 below. In this situation, the buoyancy force acting from B_1 creates a righting moment around G that forces the vessel back to an upright position, which is referred to as positive stability. It is important to note that the centre of gravity is assumed to be fixed in this case, which implies that there is no shifting of loads or fluids in the vessel. Furthermore, the location of the centre of gravity is determined by the distribution of mass of the object.

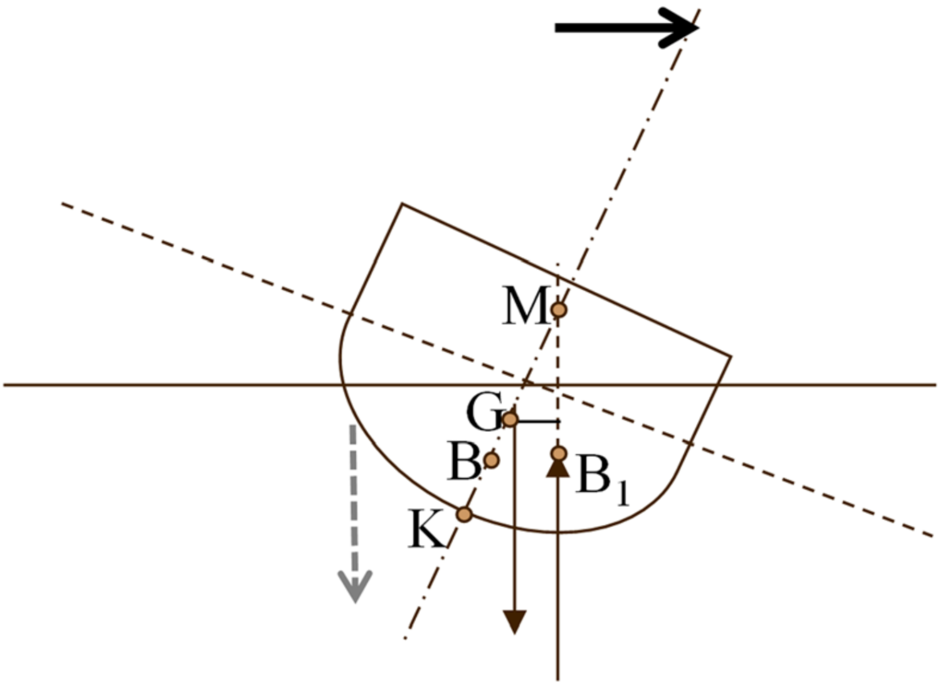

Figure 2.2: Hydrostatic stability overview (Thiagarajan and Dagher 2014)

From Figure 2.2, it can be reasoned that an unstable situation arises when $GM > 0$ is not satisfied. This negative stability arises when the centre of gravity is located above the metacentre, which causes a heeling moment that can capsize the vessel. The unstable situation can be seen in Figure 2.3 below.

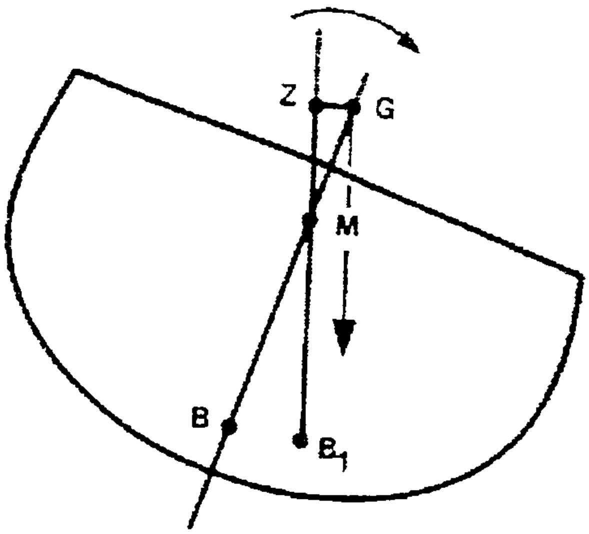

Figure 2.3: Negative stability (FAS 2008)

2.3 Stability

The concept stability has been delineated, in order to understand the definition of stability within the context of this research project. A tree diagram regarding the concept of stability can be seen in Figure 2.4 below. Stability can roughly be grouped in intact and damaged stability (Konovessis, Chua, and Vassalos 2013). Intact stability concerns the stability during normal operations of a vessel or other floating structures. Damaged stability involves for instance the stability of a vessel in a flooding condition. It has been decided that damaged stability is not taken into account. Furthermore, stability can be grouped according to static and dynamic stability. An example of dynamic stability includes, for instance, the movement of weight, such as ballast. Moreover, it includes the influence of wind on the stability of a floating structure (Molland 2011). Besides wind, Collu et al. (2014) also recognise waves and currents as loads that affect the stability of a floating wind turbine. In contrast, the static stability concerns the hydrostatic characteristics of the given structure. The green dots in Figure 2.4 indicate what has been taken into account for this research project regarding stability.

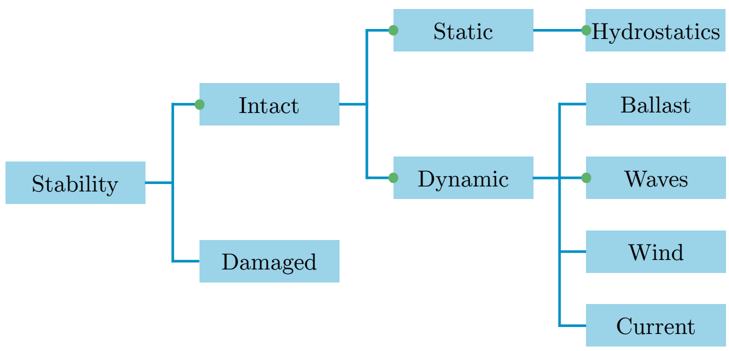

Figure 2.4: Delineation of the concept stability

3 Problem Definition

3.1 Problem context

Recent explorations within the offshore wind industry have been focused on moving wind turbines further offshore in order to harness the significant potential energy present at open oceans. In fact, it has been estimated that solely the wind resource potential located 5 to 50 nautical miles off the US coast could provide the total electrical generating capacity of 900 GW currently installed in the USA (Failla and Arena 2015). Along with wind energy, the harnessing of wave energy is a research topic that has received renewed interest due to concerns regarding global warming (Muetze and Vining 2006). Since wind and waves occur in harmony at sea, a recent research subject has emerged, which concerns the combined exploitation of the significant wave and offshore wind energy potentials (Pérez-Collazo, Greaves, and Iglesias 2015). The possible synergy of capturing both wind and wave energy in a single hybrid system is of significant interest to Ocean Grazer for future business opportunities. However, in order to harness the potential energy further offshore, a floating structure must be used since, at depths larger than 60 m, a fixed structure would not suffice in terms of feasibility (Failla and Arena 2015). Although a floating structure is preferred in large water depths, a number of challenges still remain. One of the main challenges involved with a floating wind turbine platform is regarded to be the stability with respect to wave and wind induced motions, especially during storms (Liu et al. 2016). When a wind turbine is subjected to unstable motion, energy production targets may not be met and, more importantly, large movements can result in unreliability and ultimately the sinking of a construction (Yang et al. 2019). Presently, Ocean Grazer has a conceptual design idea for a Floating Hybrid Wind-Wave Platform (FHWWP). Nonetheless, Ocean Grazer is currently unaware whether the floating structure is stable.

3.2 Problem owner

Marijn van Rooij is the problem owner of this research project. Marijn is a co-founder of Ocean Grazer and CTO, and is thus primarily responsible for the technological developments of the company. Therefore, he wishes to investigate the possibility for Ocean Grazer to develop the FHWWP. Consequently, he has a stake in a potential beneficial outcome of this research project since knowledge on the stability of the conceptual platform design would provide insights on whether to continue or possibly halt the development. Throughout the research, weekly meetings will take place in order to ensure that the research is properly scoped and delivers the intended results.

3.3 Stakeholder analysis

Besides the problem owner, other stakeholders have been identified. The role of each stakeholder in this research has especially been determined and possible conflicts have been considered.

- **Wout Prins**: Wout is a co-shareholder of Ocean Grazer and is the main inventor of the company and its concepts. Wout has initially discussed the idea of a FHWWP with Marijn and shows significant interest in the concept. Furthermore, Wout also has a stake in a beneficial outcome of this project, as it can expand the technical capabilities of the company. The stake in this project of Wout is aligned with Marijn and therefore no conflicts in incorporating both stakes are expected. Even though Wout is not able to attend the weekly meetings due to personal reasons, the progress of the research will be reported to him at least weekly.
- **Customers and investors**: Customers such as energy companies and investors have a potential stake in a beneficial outcome of this project. For instance, if computer simulations show that the new platform design is in fact stable, it positively affects the feasibility of a hybrid floating platform technology, thus signalling a promising investment. For this reason, customers and investors could exhibit some interest in the research, although it is expected at a later stage in the development.
- **Competitors**: Finally, competitors could be identified as potential stakeholders. However, it is determined that competitors are likely to become a stakeholder once the hybrid platform concept has become a feasible product. Therefore, in terms of this research, competitors are not considered as active stakeholders. Nonetheless, knowledge generated by competitors in terms of stability might be used throughout the project.

3.4 System description

A system description has been developed in order to provide an overview on the elements involved in the object of study, while highlighting the scope of the project. The system diagram can be seen in Figure 3.1 and each aspect has been elaborated in the sections below.

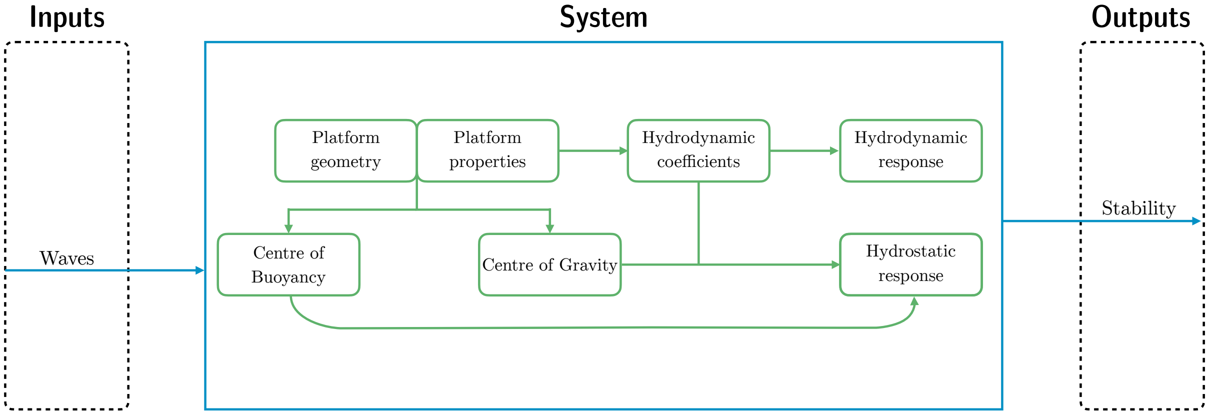

Figure 3.1: System description

3.4.1 System

It is deemed imperative to first introduce the system of study itself, which is the FHWWP. The conceptual design that has been provided by the problem owner can be seen in Figure 3.2. Initially, the FHWWP has been conceptualised for usage in the North Sea. In accordance with the stakeholders, it is assumed that the platform will only be facing the direction of the incoming waves.

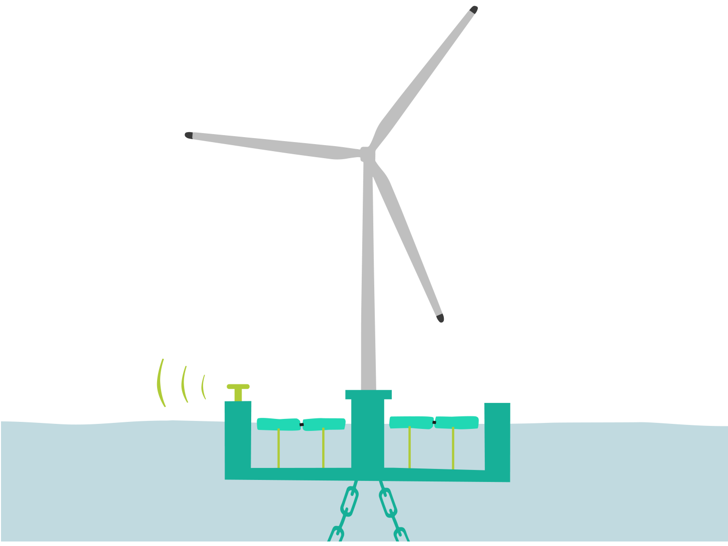

Figure 3.2: Conceptual platform design

In essence, the structure consists of three parts, which have been shown in Figure 3.3 below from a front facing perspective.

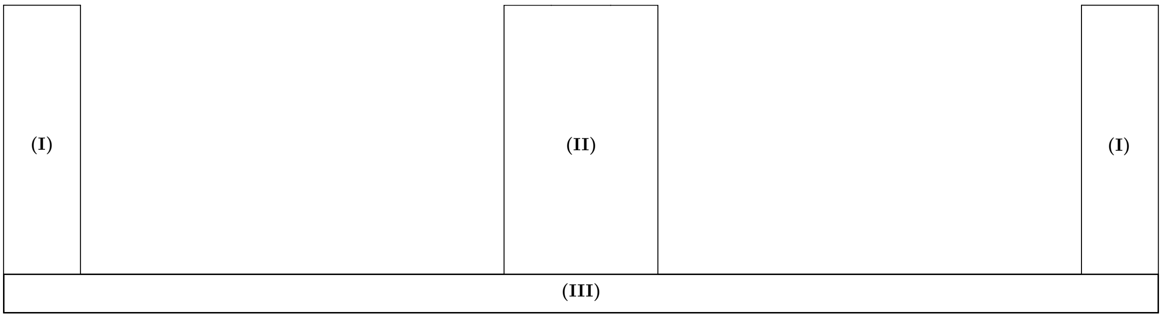

Figure 3.3: Parts of the platform structure: left & right columns (I), middle column (II) with twice the width of (I) and a horizontal plate that houses WEC equipment (III).

Moreover, the face of the platform is depicted as being flat. However, a more aerodynamic shape might have a significant impact on the response of the platform. Therefore, the problem owner Marijn and stakeholder Wout have expressed the interest in an analysis on the effect of a round bow shape. Furthermore, Figure 3.2 includes mooring cables connected to the bottom of the FHWWP. Although mooring is an important stabilising mechanism, that ensures that a floating structure remains in a fixed position, it is neglected throughout the analysis. This has been decided in order to ensure that the research can be completed successfully. In Figure 3.1, the elements of interest and the interrelations within the system regarding stability have been portrayed. The properties and geometry of the FHWWP are suspected to have a significant impact on both the hydrodynamic response to the waves and the hydrostatic response. The impact on both responses are transmitted through certain hydrodynamic coefficients, which are to be determined for the platform.

3.4.2 Inputs

The inputs that interact with the system, have been defined to be solely waves. Although wind is expected to have a significant impact on the stability and response of the FHWWP, it is nonetheless neglected for simplification purposes. The stakeholders have expressed that the initial location of deployment of a FHWWP is the North Sea. Therefore, in a real life setting, the platform is expected to encounter oceanic waves. Oceanic waves are irregular and can be approximated using a linear superposition of wave components. However, in order to determine the response of the system in this research, the waves are confined to be regular waves. The following is a brief description of regular waves.
Regular, or harmonic, waves can be defined as planar sinusoidal waves (Massie and Journée 2001). A schematic overview can be seen in Figure 3.4 below.

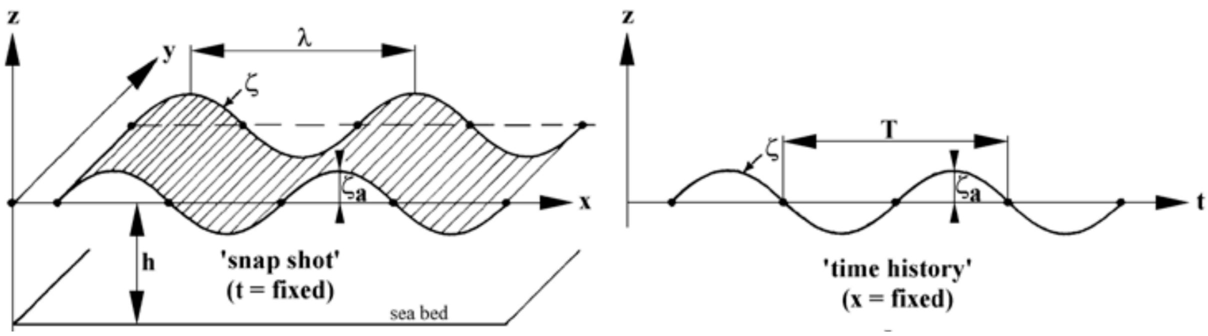

Figure 3.4: Regular waves (Massie and Journée 2001)

Several parameters of this type of wave have been specified. The highest point on a wave is the crest, whereas the lowest point on the surface is the through, both at an equal distance from the still water level. The distance in this case is equal to the amplitude ζ_a. Consequently, the water depth h is defined as the distance from the still water level to the sea bed. The height of a wave H has been defined as follows:

$$H = 2\zeta_a \tag{3.1}$$

Furthermore, the horizontal distance between two successive wave crests is the wavelength λ. This distance along the time axis is the wave period T. Since sine and cosine waves are expressed in terms of angular arguments, the wavelength and period are converted to angles:

$$k = \frac{2\pi}{\lambda} \tag{3.2a}$$

$$\omega = \frac{2\pi}{T} \tag{3.2b}$$

where k is the wave number rad/m and ω is the wave frequency rad/s. Since the waveform moves one wavelength during a period, the speed, or phase velocity c, has been determined as:

$$c = \frac{\lambda}{T} = \frac{\omega}{k} \tag{3.3}$$

For a wave moving in the positive x direction, the wave profile can be expressed as follows:

$$\zeta = \zeta_a \cos\left(kx - \omega t\right) \tag{3.4}$$

with x in m and t in s.

3.4.3 Outputs

Finally, the output has been defined as stability, determined by the response of the FHWWP. In chapter 2, a delineation of the concept stability has been proposed. Based on this delineation, the output of the system can be defined as the hydrostatic and hydrodynamic stability as a result of wave induced motions. In short, the hydrostatic and hydrodynamic response will indicate whether the FHWWP will remain in an upright position under the influence of waves.

3.5 Problem statement

The problem statement has been derived using a why-what model. The model examines the original problem at hand by first considering the broader problem: why does the problem need to be solved? Secondly, the narrow issue is examined: what is stopping the company from solving the problem? By means of the model, the following problem statement has been obtained:

> Currently, Ocean Grazer is unaware of how stable the conceptual platform design is under the influence of wave induced motions. Ultimately, the uncertainty may impede new business opportunities and the potential to expand the renewable technologies, which can threaten the competitiveness of the company.

3.6 Research Objective

Based on the problem definition and insights from the stakeholders within Ocean Grazer, an objective of the research has been formulated as follows:

> The goal of this project is to assess whether the stability of the conceptual hybrid floating platform design is sufficient, by studying the response of the system to wave induced motions, which is to be completed within a time span of three months.

The time bound of three months has been based on the fact that the project is to be completed within this time span. Therefore, it is possible that the scope and complexity of the project can be influenced by the fixed time frame.

3.7 Research questions

In order to achieve the research objective that has been introduced in section 3.6, research questions have been developed. One main research question has been formulated which is to be answered through five sub-questions seen below. The exact deliverables and methods to obtain it have been further defined in chapter 4 Methodology.

1. To what degree is the conceptual platform design sufficiently stable under the influence of wave induced motions?
    (a) What are the equations of motion of the floating platform?
    (b) What are the design characteristics of the floating platform?
    (c) What are the hydrodynamic coefficients of the floating platform?
    (d) What is the hydrostatic response of the floating platform?
    (e) What is the hydrodynamic response of the floating platform to regular waves?

4 Methodology

4.1 Overview

Based on the research questions that have been formulated, five deliverables of this research project have been defined. Each deliverable and accompanying method, including the strategy, sources, how they are accessed and the tools, have been summarised in Table 4.1 below. It is worth mentioning that the research questions connected to the deliverables have been ordered based on the sequence of the answering of the respective questions throughout the research. An elaboration on the methods in terms of theory and tools has been provided in the following sections.

Research question	Deliverable	Strategy	Sources	Access	Tool
Sub (a)	n/a	Desk research	Literature	Search methods	Literature databases
Sub (b)	(1) Platform design embodiment	Desk research	People	Questioning	Solidworks
Sub (c) Sub (d)	(2) Hydrodynamic coefficients (3) Hydrostatic response	Imitation experiments	n/a	n/a	NEMOH
Sub (e)	(4) Hydrodynamic response	Imitation experiments	n/a	n/a	MATLAB
Main (1)	(5) Stability assessment	Imitation experiments	n/a	n/a	MATLAB

Table 4.1: An overview of the methods for each deliverable

4.2 Theory

4.2.1 Linear potential flow theory

The Navier-Stokes Equations (NSE) supplemented by a conservation of mass equation form the basis of analyses regarding the dynamics of fluid motion. If viscous forces are neglected, it is feasible to construct mathematical solutions for flow past bodies (Newman 2018). Although the nonlinear NSE methods are able to provide precise prediction of WEC hydrodynamics, the approach is significantly expensive in computations (Guo et al. 2017). Moreover, due to the high complexity of the NSE, assumptions can be made for simplification. In fact, Linear Potential Theory, which is an idealised model of fluid flow, can be applied by means of the following assumptions (Payne et al. 2008):

1. The fluid is assumed to be **inviscid** and **incompressible**, meaning that it has zero viscosity and constant density respectively

2. The flow is **irrotational**

3. The **body motions are small** compared to the cross-sectional dimensions of the body

4. The **amplitude of the waves is small** in comparison to the wavelength.

A further explanation on Linear Potential Theory can be found in Faltinsen (1993) Chapter 2.

4.2.2 Equations of motion

Essentially, a floating object in the presence of waves can be described through a mechanical oscillator composed of a mass-spring-damper system undergoing a forced oscillation, which can be seen in Figure 4.1 below.

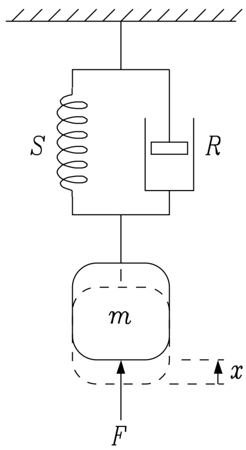

Figure 4.1: Mechanical oscillator with a mass-spring-damper system (Falnes and Kurniawan 2020)

With linearity assumed, the main forces on a floating object can be described by the excitation loads and radiation loads (ibid.). Firstly, the excitation loads entail the analysis of forces and moments when the floating structure is restrained from oscillating under the influence by the incident regular waves. These wave excitation loads are comprised of the Fraude-Kriloff and diffraction forces and moments. Secondly, the radiation loads contain the forces and moments generated when the structure is forced to oscillate while there are no incident waves. The radiation loads include forces generated by the motions of the structure itself, which includes an added mass and hydrodynamic damping term. The added mass can be thought of as a particular volume of the fluid surrounding the structure, which is accelerated as a result of the motions (Newman 2018). The damping term corresponds to damping that occurs as the motions of the structure generate waves in the surrounding fluid. Additionally, a restoring load intends to return the floating structure to the steady state position. In this project, linearity is assumed. Therefore, the excitation and radiation forces can be added in order to obtain the total hydrodynamic forces (Faltinsen 1993), which can be seen in Figure 4.2.

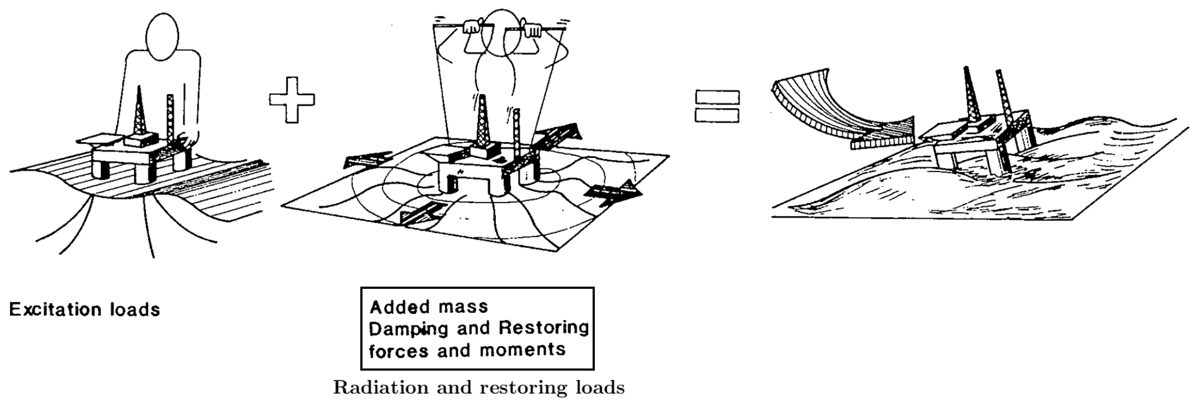

Figure 4.2: Hydrodynamic loads acting on a floating structure, adapted from Faltinsen (1993)

In order to describe the response of the FHWWP, it has been chosen to approximate the motions comparable to a WEC, where the platform is a free floating object under the influence of incident regular waves. In general, the equations of motion can be written by summing all forcing acting on a body, then applying Newton's second law (4.1) (Nolte and Ertekin 2014):

$$\sum F = m\ddot{z} \tag{4.1}$$

where m is the body mass, $\ddot{z}$ is the body acceleration in one DOF and $\sum F$ the sum of forces acting on the body. By adapting the equations of motion described by Wei et al. (2019) for a single free floating object in one DOF, the following expression is obtained:

$$m\ddot{z} = F_{ex} + F_{rad} + F_{hs} \tag{4.2}$$

with F_{ex} the frequency dependent excitation force due to the incident waves. The remaining forces are defined further. The radiation force F_{rad} is described through the added mass m_a and hydrodynamic damping b term, which can be written in the following form (ibid.):

$$F_{rad} = -m_a(\omega)\ddot{z} - b(\omega)\dot{z}. \tag{4.3}$$

The added mass and hydrodynamic coefficients are frequency dependent and are only a function of the body surface geometry that is in contact with the surrounding fluid; the wetted surface area (Ansys 2014).

F_{hs} is the restoring force that arises when the body is moved away from the equilibrium position, which is comprised of the buoyancy force F_B and the gravitational force F_g. It can be written in the following form (Wei et al. 2019):

$$F_{hs} = -k_{hs}z \tag{4.4}$$

where k_{hs} is the hydrostatic stiffness coefficient, which specifies the variation of the gravitational and buoyancy force as the position changes with respect to the equilibrium. The stiffness coefficient is not a function of wave frequency; it is solely a function of the cross-sectional area of the object at the still water line and it can be regarded as analogous to the spring in Figure 4.1.

It is imperative to note at this point that drag forces have not been considered. Essentially, it can be argued that for large structures, the drag force can be neglected, as opposed to the inertial forces. In fact, Zhang and Paterson (2015) have shown that the magnitude of the drag force for a large yet simple floating wind-turbine structure is negligible in comparison to the magnitude of the inertial force. For the purpose of this research project, the findings of negligible drag force have been extended to apply to the FHWWP in this case.

By combining equations (4.3) and (4.4) into (4.2) and rearranging the expression, the following has been obtained:

$$(m + m_a(\omega))\ddot{z} + b(\omega)\dot{z} + k_h z = F_{ex}. \tag{4.5}$$

The vector for displacement, velocity and acceleration can be expressed in the following way:

$$z = \begin{bmatrix} z \\ \dot{z} \\ \ddot{z} \end{bmatrix}. \tag{4.6}$$

It is imperative to note that the vector in (4.6) can be expressed in both time-domain and frequency-domain. For the purpose of this project, the system is placed in the frequency-domain. In fact, Jurado, Borg, and Bredmose (2018) denote several advantages of frequency-domain analyses such as; faster computation times, solutions can be obtained relatively quickly and easier handling of frequency-dependent parameters, compared to time-domain analyses. Since all parameters in (4.5) are either constant of frequency dependent, the system has been placed in the frequency domain in the following way (ibid.):

$$z = \begin{bmatrix} z(t) \\ \dot{z}(t) \\ \ddot{z}(t) \end{bmatrix} = \begin{bmatrix} \hat{z}(\omega)e^{i\omega t} \\ i\omega\hat{z}(\omega)e^{i\omega t} \\ -\omega^2\hat{z}(\omega)e^{i\omega t} \end{bmatrix} \tag{4.7}$$

and

$$F_{ex}(t) = \hat{F}_{ex}(\omega)e^{i\omega t}. \tag{4.8}$$

It is then possible to adapt (4.5) to the following form:

$$[-\omega^2(m + m_a(\omega)) + i\omega b(\omega) + k_h]\hat{z} = \hat{F}_{ex}. \tag{4.9}$$

Since the above expression is valid for one DOF, it has been altered to represent the motion in six DOF:

$$[-\omega^2(\mathbf{M} + \mathbf{M}_a(\omega)) + i\omega\mathbf{B}(\omega) + \mathbf{K}_h]\hat{\mathbf{Z}} = \hat{\mathbf{F}}_{ex} \tag{4.10}$$

where $\hat{\mathbf{Z}}$ is the 6x1 displacement vector in the six DOF: surge, sway, heave, roll, pitch and yaw. $\mathbf{M}$ is the 6x6 mass matrix containing the platform mass and moments of inertia, with the following structure:

$$\mathbf{M} = \begin{bmatrix} m & & & & & \\ & m & & & & \\ & & m & & & \\ & & & I_{xx} & I_{xy} & I_{xz} \\ & & & I_{xy} & I_{yy} & I_{zy} \\ & & & I_{xz} & I_{yz} & I_{zz} \end{bmatrix}. \tag{4.11}$$

$\mathbf{M}_a$ is the 6x6 frequency dependent added mass matrix. Correspondingly, $\mathbf{B}$ is the 6x6 frequency dependent hydrodynamic damping matrix. It is common to obtain the added mass and damping matrices through computer software, since both matrices are significantly difficult to obtain analytically. $\mathbf{K}_h$ is the 6x6 hydrostatic stiffness matrix, with the following structure:

$$\mathbf{K}_h = \begin{bmatrix} 0 & 0 & 0 & 0 & 0 & 0 \\ 0 & 0 & 0 & 0 & 0 & 0 \\ 0 & 0 & K_{h33} & K_{h34} & K_{h35} & 0 \\ 0 & 0 & K_{h34} & K_{h44} & K_{h45} & 0 \\ 0 & 0 & K_{h35} & K_{h45} & K_{h55} & 0 \\ 0 & 0 & 0 & 0 & 0 & 0 \end{bmatrix}. \tag{4.12}$$

Since the platform is considered to be a free-floating body, $\mathbf{K}_h$ should be a symmetric matrix, as shown in (4.12) (Ansys 2014). Furthermore, it should be noted that only the motions heave, roll and pitch contribute to the stiffness matrix. This is due to the fact that only these motions displace the centre of gravity or alter the submerged volume, which has en effect on the buoyancy force respectively. By analysing the hydrostatic stiffness matrix, conclusions can be drawn on the static stability of the object. For instance, if the diagonal entry K_{h44} is a positive value, it infers that a roll motion will not generate a heeling moment that capsizes the object. Finally, $\hat{\mathbf{F}}_{ex}$ is the 6x1 excitation force vector. It is possible to obtain $\mathbf{M}$, $\mathbf{M}_a$, $\mathbf{B}$, $\mathbf{K}_h$ and $\hat{\mathbf{F}}_{ex}$ from the open source software NEMOH, which has been further elaborated in section 4.3.

4.2.3 Response Amplitude Operator

The Response Amplitude Operator (RAO), can be defined as the harmonic response of a floating body to regular waves (ibid.). With the equation of motions given in (4.10), the RAO for each DOF can be obtained the following way:

$$\mathrm{RAO}(\omega) = \hat{\mathbf{Z}} = \mathrm{H}\hat{\mathbf{F}}_{ex} \tag{4.13}$$

with

$$\mathrm{H} = [-\omega^2(\mathbf{M} + \mathbf{M}_a(\omega)) + i\omega\mathbf{B}(\omega) + \mathbf{K}_h]^{-1}. \tag{4.14}$$

In essence, H can be referred to as the transfer function of the system which relates the input force to the output response. In this case, $\hat{\mathbf{F}}_{ex}$ only consists of the first order wave excitation force induced by a regular wave with the unitary amplitude of 1 m (ibid.). The RAO is then proportional to the regular wave amplitude. Therefore, the results of the RAO computations reflect the actual translation and rotation in the six DOF. Equations (4.13) and (4.14) form the primary equations that are solved in order to derive the frequency-domain response $\hat{z}$ of the FHWWP. Since $\hat{z}$ is a complex term, the displacement RAO can be obtained by computing the argument of this term.

4.2.4 Natural frequency

The natural frequency ω_n in rad/s of an object can be used in order to verify potential peaks that may occur in the RAO of certain DOFs. Based on the expression presented by Vantorre, Banasiak, and Verhoeven (2004), ω_n can be obtained using the following expression:

$$\omega_n = \sqrt{\frac{\mathbf{K}_h}{\mathbf{M} + \mathbf{M}_a(\omega_n)}} = \omega \tag{4.15}$$

where by subtracting the frequency ω, ω_n can be determined at the zero crossing: $\omega_n - \omega = 0$. It is imperative to note that for determining the natural frequency of a certain motion, the corresponding coefficients for that DOF must be chosen from the matrices $\mathbf{K}_h$, $\mathbf{M}$ and $\mathbf{M}_a$. Once the wave frequency is equal or close to the natural frequency, resonance occurs which in turn increases the amplitude of motion, resulting in a significant peak in the RAO. Essentially, since heave, roll and pitch are subject to the hydrostatic stiffness, there exists a natural frequency at which the structure can oscillate in those three DOF, which is to be avoided (Aird 2018).

4.2.5 System stability

The stability of a system can be determined by analysing the transfer function that describes the system. A transfer function $H(s)$ is defined in the s-domain, where s is a complex number in the form $s = x + i\omega$. Generally, a transfer function has the following form:

$$H(s) = \frac{N(s)}{D(s)} \tag{4.16}$$

where $N(s)$ and $D(s)$ are polynomials. The roots of $N(s)$ are defined as zeros, which indicate the value for which the transfer function equals zero. Likewise, the roots of $D(s)$ are defined as poles, that indicate the value for which the transfer function tends to infinity. The locations of poles and zeros can be plotted in the complex plane, which in turn provides an insight on the stability of the system as described by the transfer function, which can be seen in Figure 4.3 below.

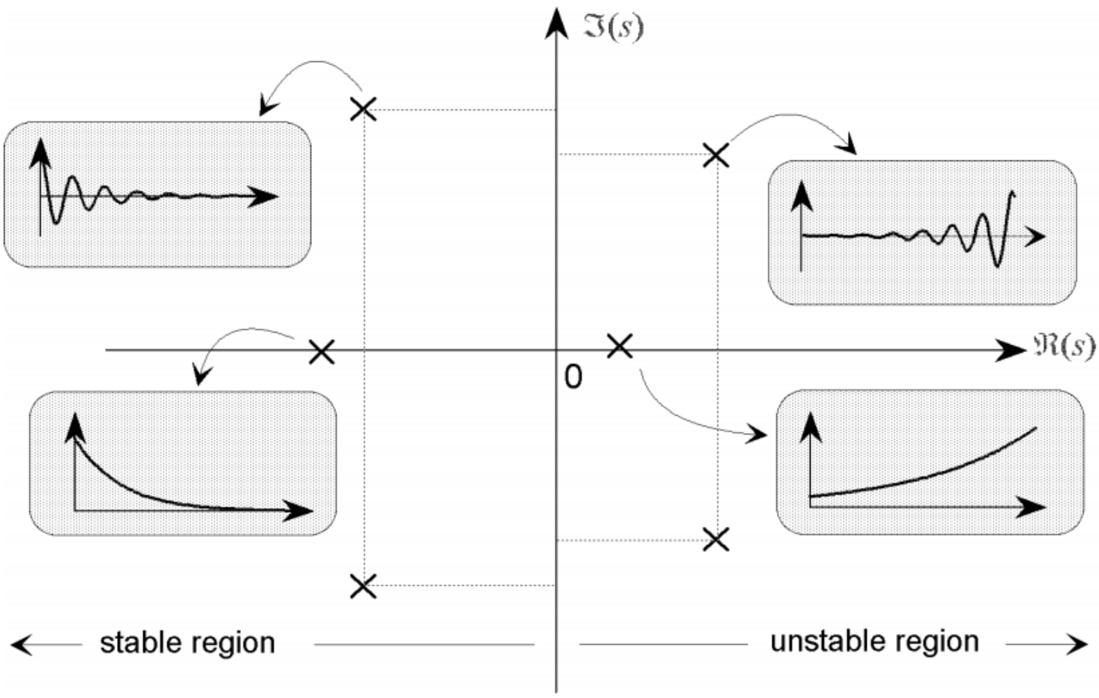

Figure 4.3: The effect of poles location on response stability (MIT 2020)

In essence, the location of the poles influences the behaviour of the response signal. This is due to the fact that in the time-domain, the poles are represented by exponential terms that affect the shape of the response signal. Firstly, the location of the poles on the imaginary axis determines the oscillatory nature of the signal. Secondly, the location on the real axis determines whether the signal is stable in nature. Therefore, as seen in Figure 4.3, poles that are situated in the Right Hand Plane (RHP) result in an increasing oscillating unstable signal. Moreover, if a pole is situated on the real axis in the RHP, the magnitude of the non-oscillating signal increases likewise, which results in instability. Consequently, the system is stable when the poles are situated either on the imaginary axis or in the Left Hand Plane (LHP).

4.3 Tools

In order to obtain answers to the research questions and results for the deliverables, several tools such as software programmes have been used for the computations and analysis. An overview on the applied tools at each stage can be seen in Figure 4.4 below.

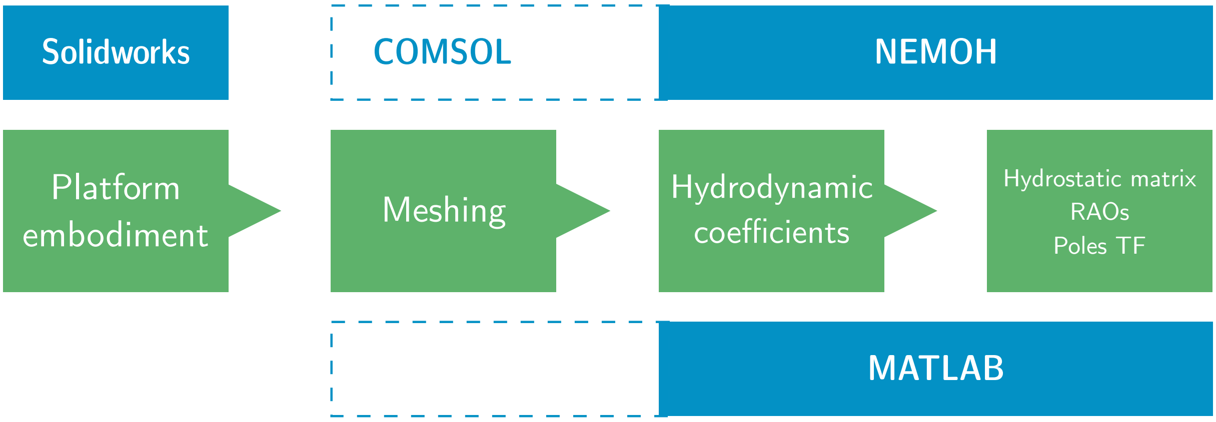

Figure 4.4: The applied tools in the analysis process

4.3.1 Solidworks

The platform embodiment has been constructed in the Computer Aided Design (CAD) software Solidworks. This software allows for the creation of three-dimensional objects which can then be analysed in several physical studies. However, for the purpose of this project, Solidworks has been solely used in order to obtain a three-dimensional model of the FHWWP, along with important characteristics such as the centre of gravity.

4.3.2 COMSOL

COMSOL is a multi-physics and finite element analysis simulation software, which is often used for modelling and simulating scientific and engineering problems. Comparable to Solidworks, COMSOL has not been used for physical studies. The embodiment obtained from Solidworks has been meshed in COMSOL in order to obtain the coordinates that describe the three dimensional platform. Thereafter, the mesh has been prepared for usage in NEMOH, through an Excel macro written by R. J. M. Zwetsloot in 2017, a former MSc student involved with Ocean Grazer at that time.

4.3.3 MATLAB

MATLAB is a numerical computing environment and programming language developed by MathWorks. MATLAB has been used as a wrapper in order to run NEMOH in this environment, which has been further elaborated in the following subsection. Furthermore, a MATLAB script has been written in order to obtain the dynamic harmonic response and process the results into plots. Finally, in order to determine the natural frequency for certain DOF, a MATLAB script has been written likewise. The utilised MATLAB scripts have been listed in Appendices A.1, A.2 and A.3 respectively.

4.3.4 NEMOH

NEMOH is an open-source Boundary Element Method (BEM) code which computes first order wave loads, in order to estimate the dynamic response of offshore floating structures (Babarit and Delhommeau 2015). The software utilises the numerical simulation model BEM, which is executed through solving Boundary Value Problems (BVPs), which is a system of ordinary differential equations with derivatives and solutions known at the boundaries. The main outputs of NEMOH include the required parameters in (4.13) and (4.14), such as the added mass and hydrodynamic damping coefficient. NEMOH is structured in three programs (ibid.):

- preProcessor: reads and prepares the body mesh and conditions
- Solver: solves the BVPs and calculates the respective outputs
- postProcessor: processes the results such that the outputs can be used in order to obtain for instance the RAO.

Although it is possible to run NEMOH independently, a MATLAB wrapper can be used in order to run the software within the MATLAB environment. The obtained mesh from COMSOL has been further refined by use of the preProcessor Mesh.m script provided by NEMOH, which requires the inputs shown in Table 4.2 below. The number of quadrangular panels and the body coordinates vector have been obtained from the COMSOL mesh after processing in the Excel macro. The centre of gravity coordinates have been obtained from the platform embodiment, which has been described in chapter 5. The translation and symmetry has been set at 0 to indicate that there is no translation and the body is symmetric in the xOz plane. Finally, the target number of panels has been doubled twice in order to determine the mesh convergence, which has been discussed in further detail in chapter 6.

Input parameter	Value	Description
nBodies	1	Number of bodies modelled
n		Number of quadrangular panels
X	Vector	Body coordinates vector
CG	(x,y,z)	Location of the centre of gravity
tX	0	Translation and symmetry indication
nfobj	800	Target number of panels after mesh refinement

Table 4.2: Input parameters for the preProcessor in the Mesh.m MATLAB script

Furthermore, the solver and postProcessor have been used through the Nemoh.m script, which requires the inputs shown in Table 4.3 below. The range of wave frequencies to be used for calculations in NEMOH has been chosen to highlight the platform behaviour at lower frequencies which corresponds to longer wave-lengths. For all simulations, the wave direction has been set at 0°, which corresponds to the positive x-direction. Finally, the depth has been set at 200 m, which corresponds to the deeper northern parts of the North Sea (Paramor et al. 2009).

Input parameter	Value	Description
w	[0.01:0.01:1.6]	Vector of wave frequencies (rad/s)
dir	0	Wave direction in degrees
depth	200	Water depth (m)

Table 4.3: Input parameters for the solver and postProcessor in the Nemoh.m MATLAB script

4.3.5 System Identification Toolbox

The System Identification Toolbox (SIT) is an application within MATLAB, suited for the purpose of constructing mathematical models of dynamic systems from measured input-output data. The input-output data in the frequency domain has been obtained from the NEMOH simulation with the excitation force as input data and the response as output data respectively. Consequently, the SIT has been used to fit a transfer function to the data. The given fitted transfer function could then be analysed in terms of the location of the poles. Firstly, the frequency data has been imported from the MATLAB variables that contain the input-output data. Consequently, the data has been estimated into a transfer function model, where the number of poles and zeros both have been initially assumed at two. The resulting poles and zeros corresponding to the obtained transfer function have been exported to a pole-zero map in the complex plane. An overview of the SIT application can be found in Appendix B.

5 Platform embodiment

Since the conceptual design of the FHWWP by Ocean Grazer consists of a two dimensional illustration, an embodiment of the platform has been constructed in order to perform the stability analysis. The following chapter describes the procedure of obtaining a three dimensional model of the FHWWP and the relevant characteristics.

5.1 Platform shape

The general shape of the platform has been defined by the conceptual design shown in Figure 3.2. Furthermore, with additional information from the problem owner Marijn van Rooij and stakeholder Wout Prins, a three dimensional design has been made by use of Solidworks. An isometric view of the design can be seen in Figure 5.1 below. The vertical pillar on the platform represents a simplified wind-turbine, which has been further elaborated in the next sub-section. Furthermore, the coordinate system that is used has been indicated, with the origin situated in the middle of the platform regarding the YX-plane, at the still water line regarding the Z-axis.

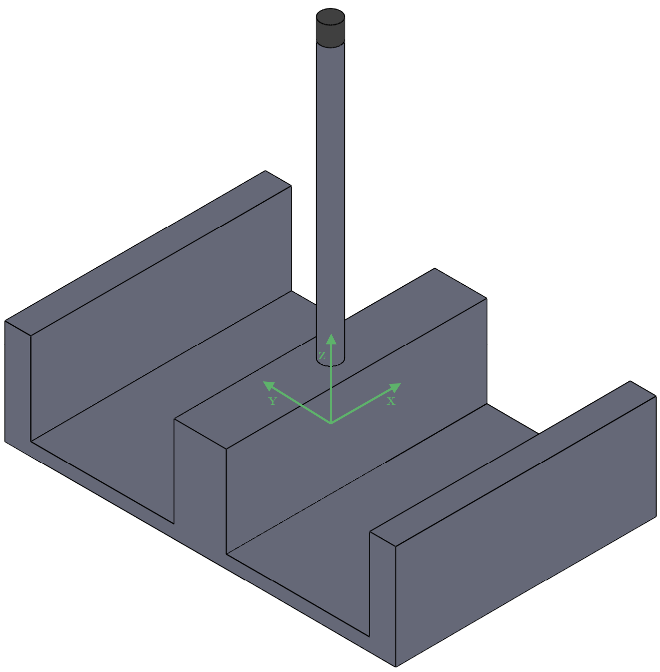

Figure 5.1: An isometric view of the platform design

The design embodiment shown in Figure 5.1, has been obtained from several assumptions regarding the intended dimensions. Firstly, the width has been assumed at 150 m. Besides, the length of the platform, which is dependent on the optimal length of the WEC floater blanket, has been defined to be 100 m. Secondly, it has been decided that the vertical columns should emerge 10 m above the still water line. Additionally, it has been determined that the platform draft is 30 m. Finally, the width of the middle column has been assumed to be twice the width of the left and right column, since a wind-turbine is mounted on this column. Therefore, the width of the middle column is 20 m, with the width of the left and right column 10 m respectively. It is important to note that the dimensions are preliminary and could be subject to change in the future development of the FHWWP. All dimensions have been indicated in Figure 5.2 below.

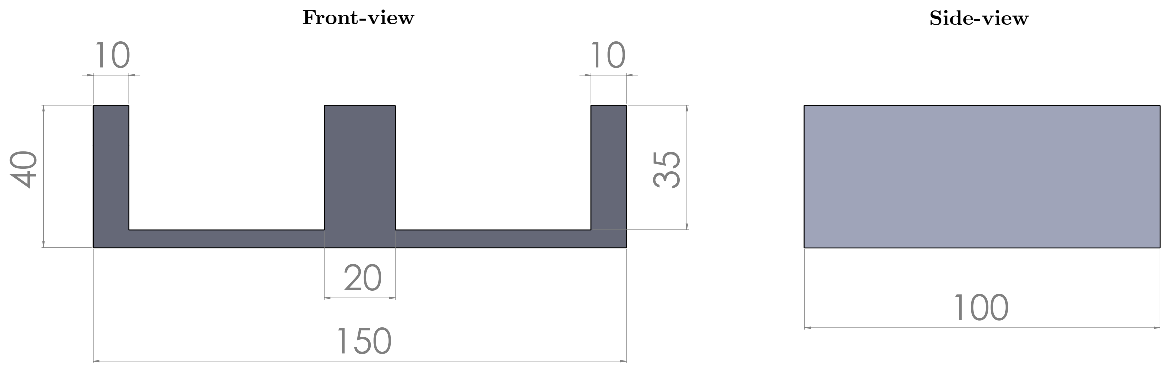

Figure 5.2: Platform dimensions in meters

5.2 Wind-turbine

In order to include a wind-turbine, an approximation has been made. In specific, the tower of the wind-turbine has been approximated as a vertical pillar with a certain constant diameter, which has been shown in Figure 5.1. For further simplification, the top part of the wind-turbine including the nacelle, a hub and three blades, has been approximated as a cylinder of equal diameter as the tower, the height of the nacelle and with the combined mass of the three components. The dimensions and mass of the different components of an 8 MW wind-turbine system have been obtained from an analysis on an equivalent reference system, performed by Desmond et al. (2016). The used characteristics have been summarised in Table 5.1 below.

Component	Mass (t)	Height (m)	Diameter (m)
Hub	90.0	n/a	n/a
Nacelle	285	7.50	n/a
Blades (3)	105	n/a	n/a
Tower	558	106	7.70

Table 5.1: Wind-turbine data (Desmond et al. 2016)

5.3 Mass and centre of gravity

Since the material and distribution of weight of the platform is not known, assumptions have been made in order to estimate the total mass and the location of the centre of gravity. Considering the fact that the horizontal plate houses the equipment for the WEC system, it has been assumed that this plate accounts for 50% of the total platform mass. Consequently, the residual mass of the platform is divided over the three vertical columns. Since the middle column is twice the size of the left or right column, it accounts for 25% of the total mass. Finally, the left and right column each account for 12.5% of the total mass.

In order to determine the total mass of the platform, Archimedes' principle (5.1) and Newton's first law in equilibrium (5.2) have been used:

$$F_B = \rho_f V_{disp} g \tag{5.1}$$

$$\sum F = 0 \Rightarrow F_B = F_g \tag{5.2}$$

where F_B is the buoyancy force in N, ρ_f the fluid density in kg/m^3, V_{disp} the displaced volume of the fluid in m^3 and g the gravitational constant in m/s^2. By combining (5.1) and (5.2), the following expression has been obtained:

$$\rho_f V_{disp} g = m_t g \tag{5.3}$$

with $m_t = m_{platform} + m_{turbine}$ as the total mass in tonnes. Through simplification, the total mass m_t is determined as follows:

$$m_t = \rho_f V_{disp} \tag{5.4}$$

The displaced volume has been obtained from Solidworks: $V_{disp} = 175 \times 10^3\,\text{m}^3$. When assuming $\rho_f = 1025\,\text{kg/m}^3$ for salt water, (5.4) has resulted in a total mass m_t of 179 375 tonnes. Since the mass of the wind-turbine $m_{turbine}$ of 1023 tonnes has been obtained from the data in Table 5.1, the platform mass $m_{platform}$ has been determined to be 178 337 tonnes.

By combining the assumptions of the mass distribution and the results of the mass calculation, the centre of gravity has been obtained from Solidworks. In terms of the proposed coordinate system in Figure 5.1, the centre of gravity is located at $(x, y, z) = (0, 0, -16.94)$. It is important to note that this is the centre of gravity of both the platform and wind-turbine combined, while taking into account the mass distribution of each component respectively. Furthermore, for both the platform and the wind-turbine, the mass is assumed to be distributed equally in each of the parts. A final summarised overview of the characteristics of the floating structure has been presented in Table 5.2.

Parameters	Value
Vertical plate dimensions	150 x 100 x 5 m
Left & right column dimensions	10 x 100 x 35 m
Middle column dimensions	20 x 100 x 35 m
Platform draft	30 m
Platform mass	178 337 tonnes
Platform displaced volume	175×10^3 m^3
Centre of gravity (combined with mass wind-turbine)	$(x, y, z) = (0, 0, -16.94)$

Table 5.2: Main characteristics platform with square bow

5.4 COMSOL mesh

In order to perform an accurate analysis on the platform embodiment, COMSOL has been used in order to obtain a mesh that sufficiently describes the geometry, which can be seen in Figure 5.3 below. The origin of the applied coordinate system is located in the middle of the platform at the still-water level. Therefore, the obtained mesh only describes the submerged area of the FHWWP. Moreover, since the geometry is symmetric in the xOz plane, it was necessary to only describe half of the structure for usage in NEMOH. Consequently, the platform has not been meshed on the top and right surfaces.

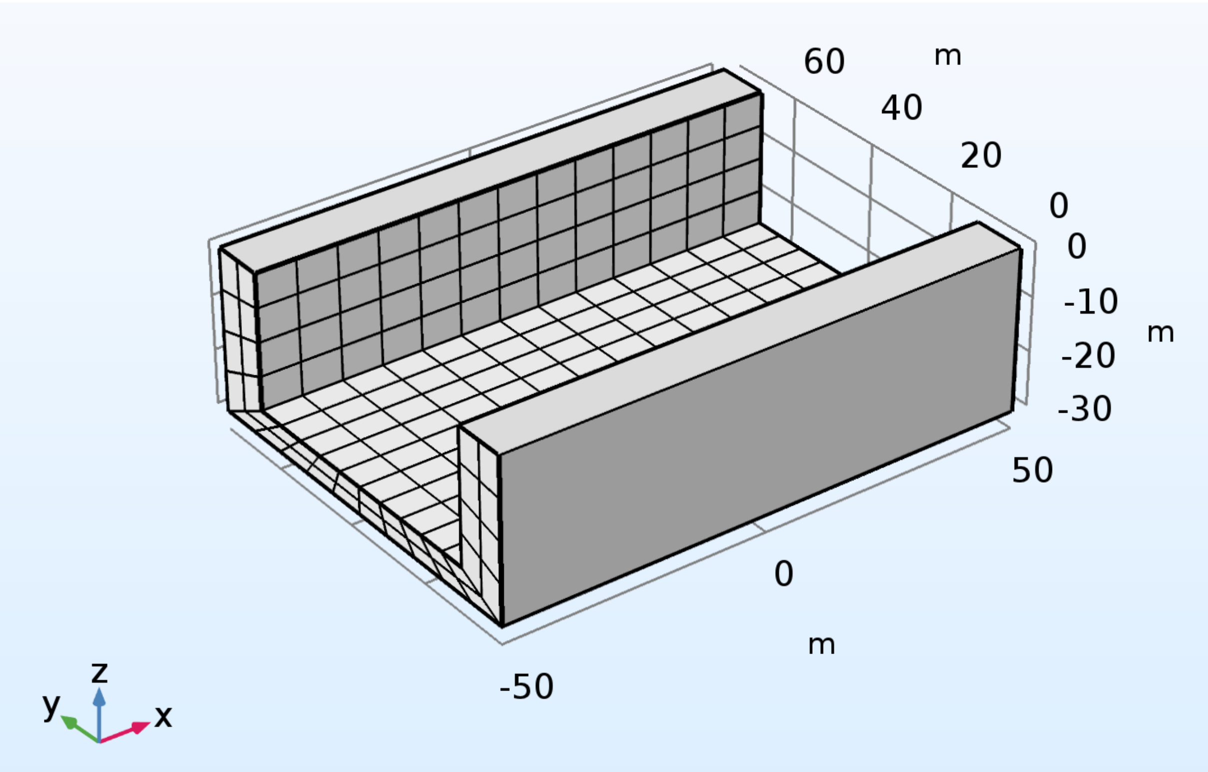

Figure 5.3: Mesh obtained through COMSOL with square bow shape

Additionally, the square bow shape seen in Figure 5.3 has been adapted to a more rounded shape in order to study the effect on the RAO and stability. This is due to the fact that it has been hypothesised by the problem owner and stakeholder that a rounded bow shape should allow water to flow through more easily. The adapted mesh can be seen in Figure 5.4 below. It is important to note that the centre of gravity has not been altered since an equal amount of mass has been added on either sides of the structure.

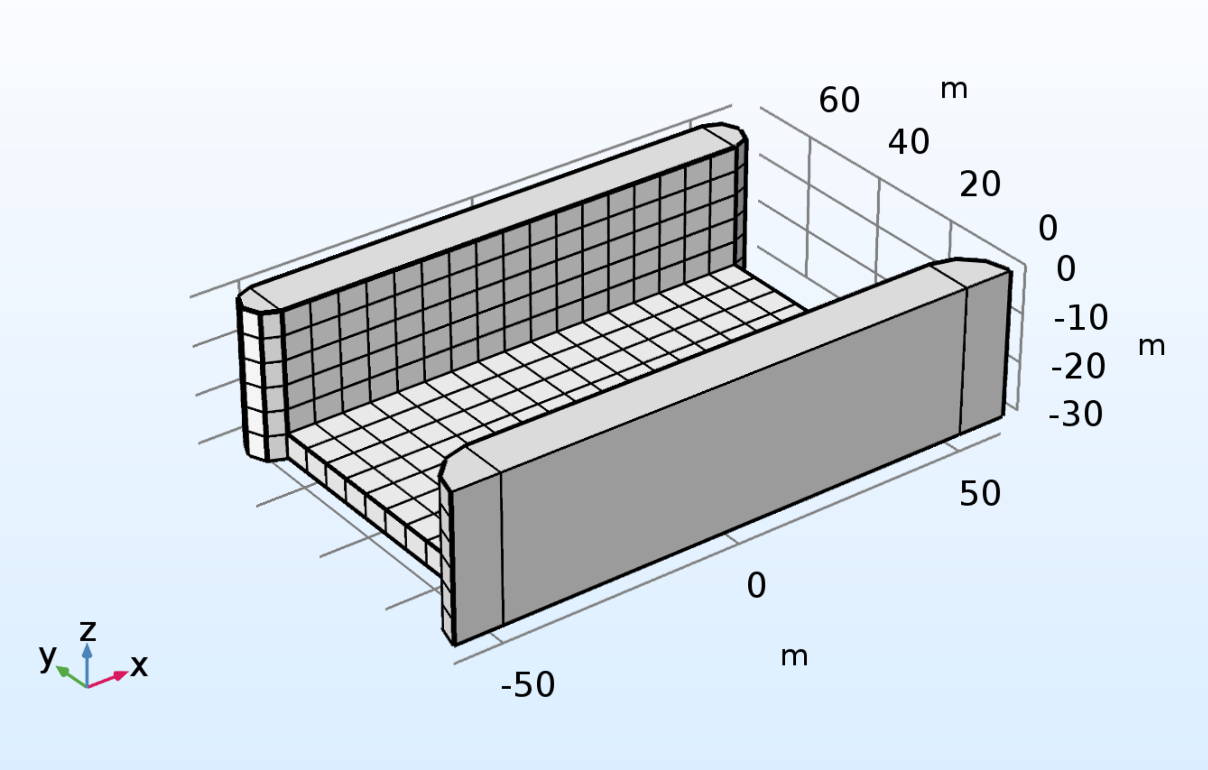

Figure 5.4: Mesh obtained through COMSOL with rounded bow shape

6 Mesh convergence

Borouchaki, Laug, and George (2000) have stressed the importance of meshing in many numerical fields. Although generally a fine mesh results in more accurate results, the computational time for each mesh refinement can increase exponentially. Therefore, a basic mesh convergence study for the square shape has been performed on the added mass in surge and pitch, in order to determine the required mesh refinement while considering the computational time. Surge and pitch have been chosen since these motions are deemed important for the rounded shape evaluation and stability assessment respectively. The COMSOL mesh has been transformed into a form which has been refined by NEMOH to a target number of panels of 800, 1600 and 3200. The obtained refined meshes can be seen in Figure 6.1, 6.2 and 6.3 respectively.

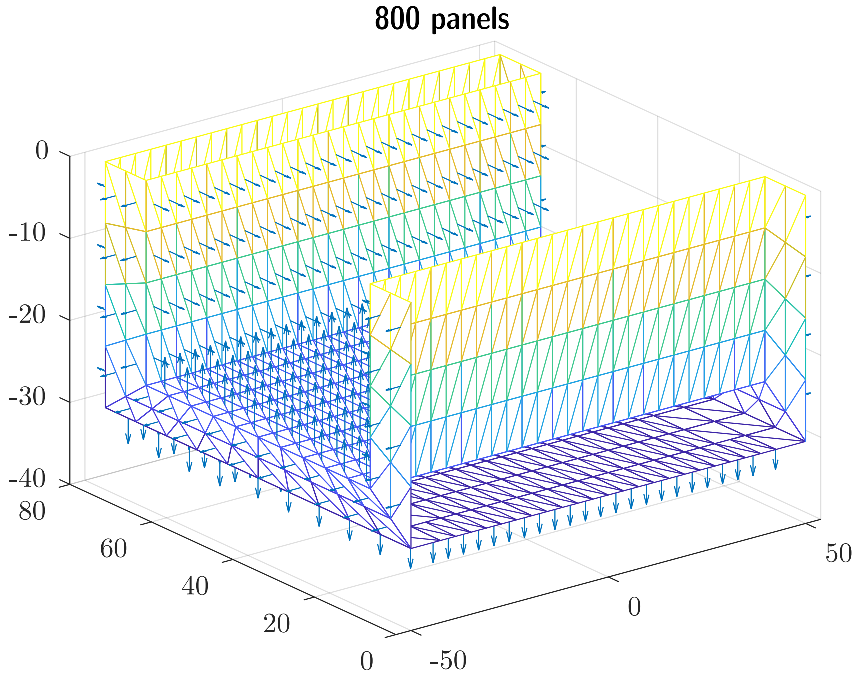

Figure 6.1: NEMOH mesh with a target number of panels of 800

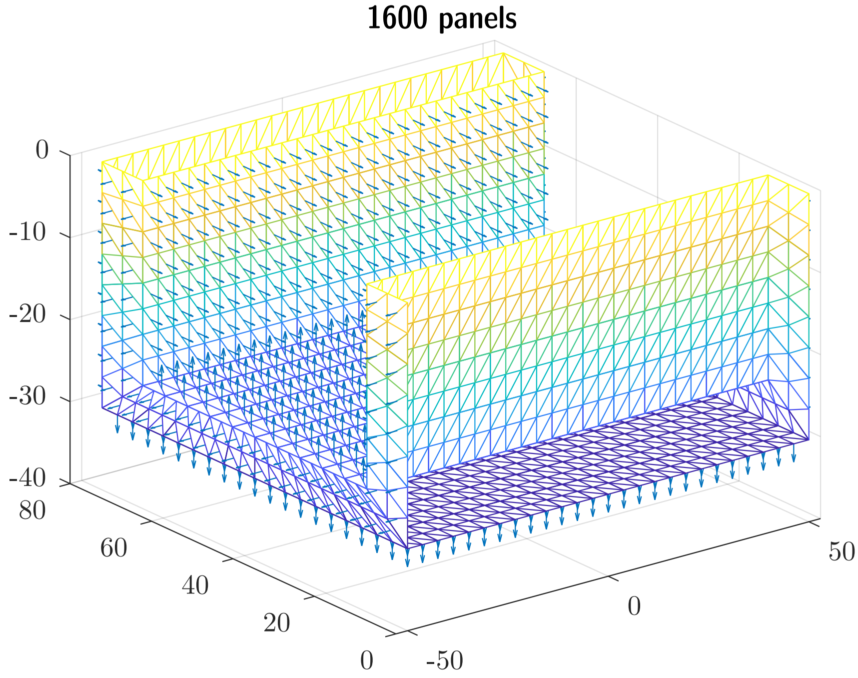

Figure 6.2: NEMOH mesh with a target number of panels of 1600

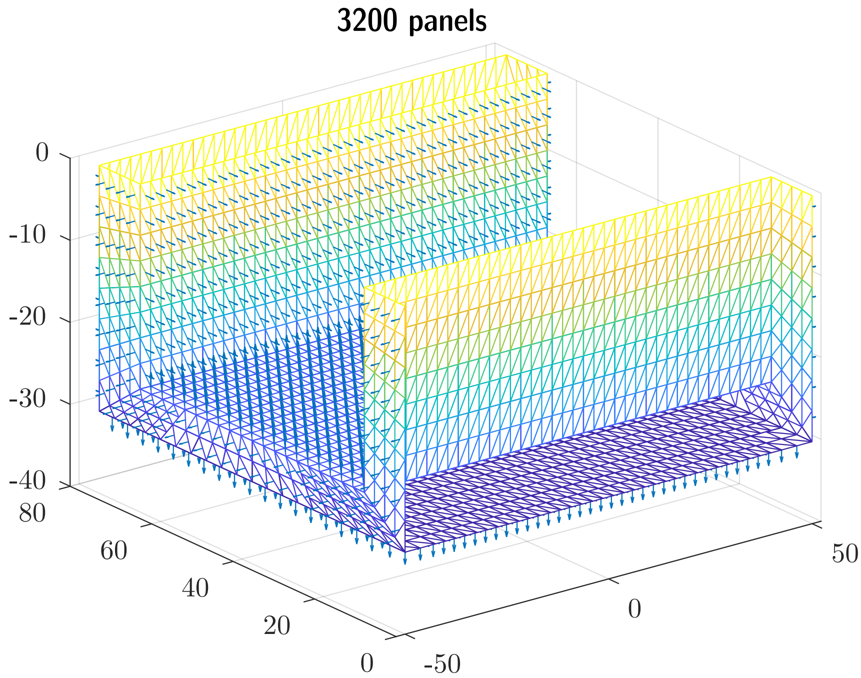

Figure 6.3: NEMOH mesh with a target number of panels of 3200

In order to evaluate the correctness of the meshes, each refinement has been assessed on whether the normal vector of each panel points towards the fluid, which is a prerequisite for the proper functioning of the NEMOH solver program. Moreover, it has been confirmed that each mesh has been fully described and does not contain holes. The results for added mass in surge and pitch for each mesh refinement has been obtained, which is shown in Figure 6.4 and 6.5 below.

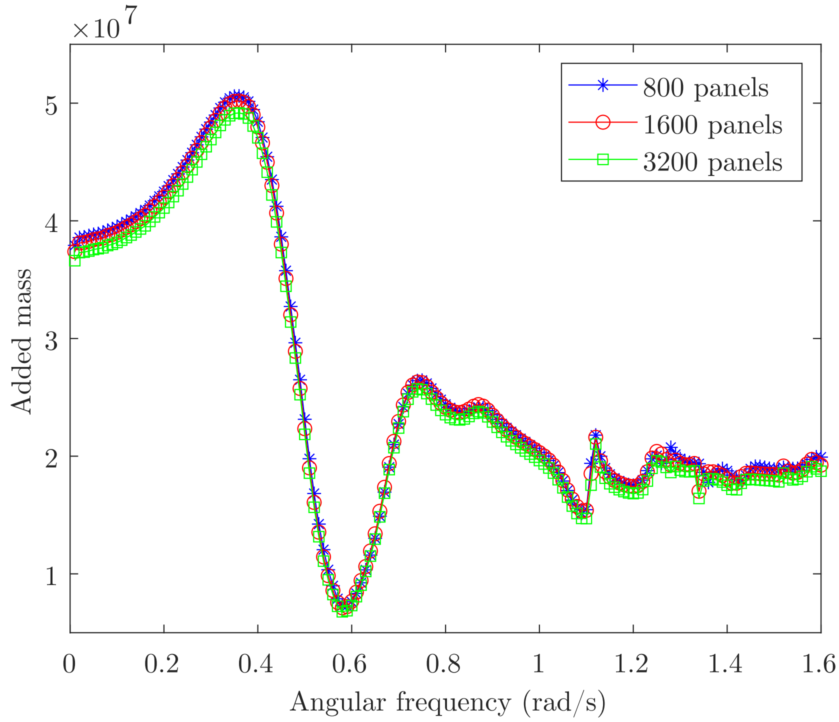

Figure 6.4: Graphical comparison of the added mass in surge for each mesh refinement

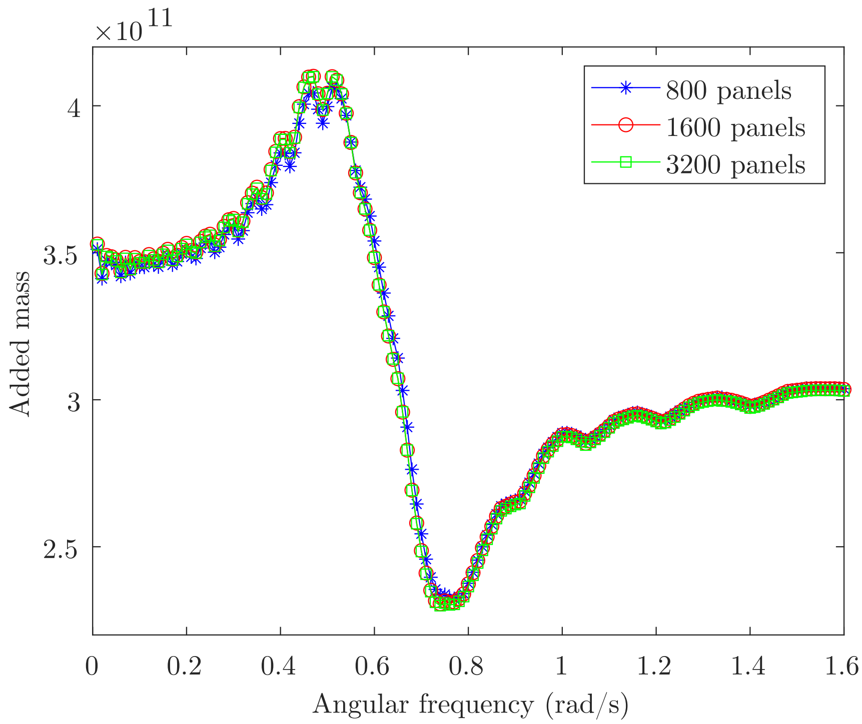

Figure 6.5: Graphical comparison of the added mass in pitch for each mesh refinement

Based on the results shown in Figure 6.4 and 6.5, the convergence error $\eta(\omega)$ at each frequency for the mesh refinements has been obtained using the following equation:

$$\eta(\omega) = \left| \frac{x_1(\omega) - x_2(\omega)}{\max(x_1)} \right| \tag{6.1}$$

where $x_1(\omega)$ is the result from the higher order mesh and $x_2(\omega)$ the result of the lower order mesh. Max(x_1) is the maximum value encountered of the higher order mesh. By multiplying the resulting $\eta(\omega)$ with 100, the convergence error percentage between the mesh refinements is obtained, which entails the percentage difference between the results. The convergence error for added mass in surge and pitch for each mesh refinement has been shown in Figure 6.6 and 6.7 respectively.

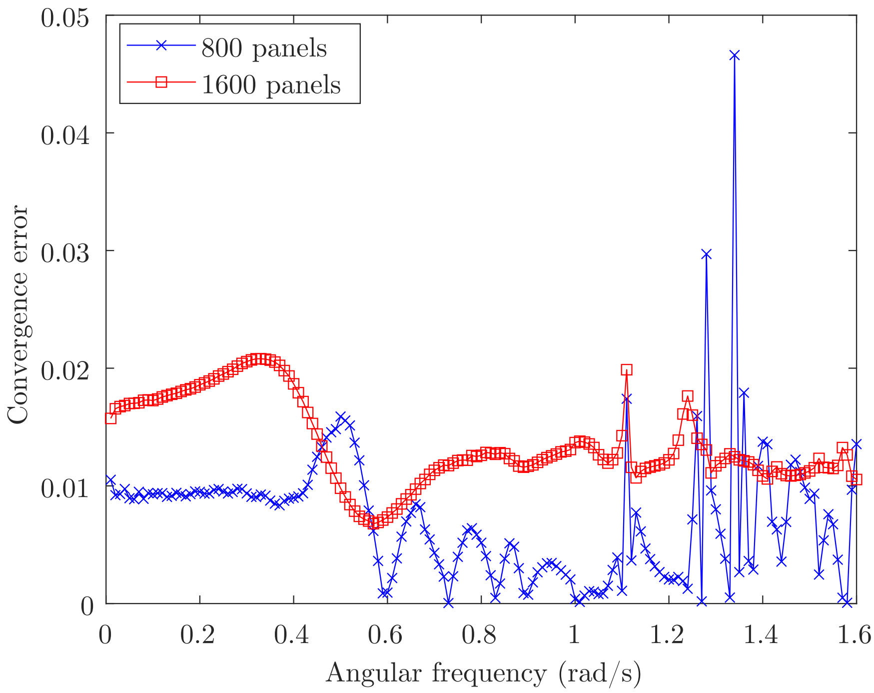

Figure 6.6: Convergence error for surge

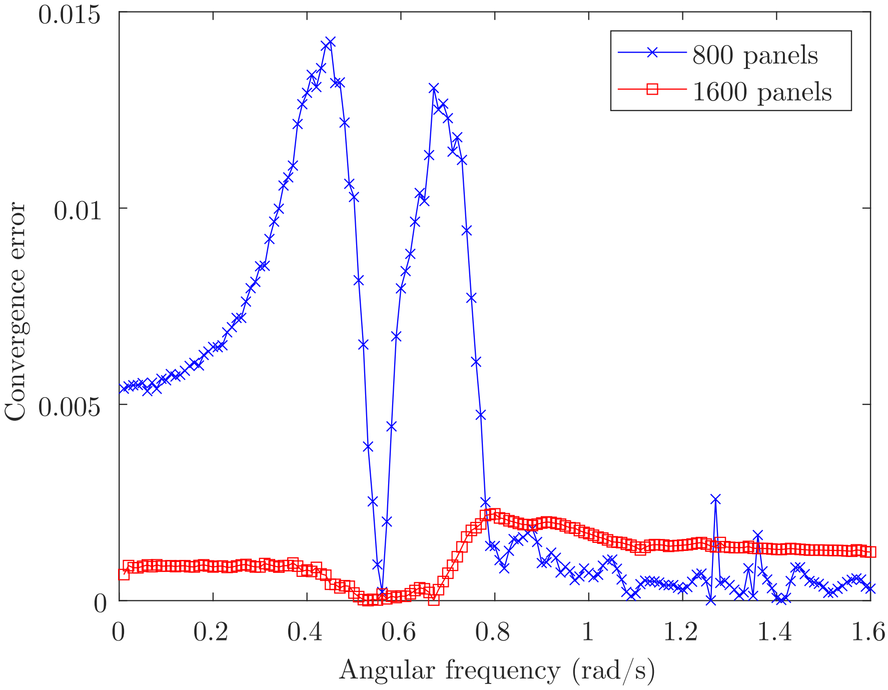

Figure 6.7: Convergence error for pitch

Through consultation with the problem owner, it has been decided that a convergence error of 5% is considered to be sufficient. For the added mass in surge, it can be seen in Figure 6.6 that the maximum convergence error between 800 and 1600 panels is roughly 0.046, or 4.6%. Furthermore, for the added mass in pitch the maximum convergence error is approximately 0.014 or 1.4%, as can be seen in Figure 6.7. Since both motions of the 800 panels have a convergence error of less than 5% and this mesh refinement has the lowest computational time, all further analyses have been based on the mesh refinement of 800 panels.

7 Results

The results for the hydrostatic and hydrodynamic response of the FHWWP for both cases of the square and round bow shape have been presented in the following chapter. The hydrostatic response has been highlighted with the hydrostatic stiffness matrix and the hydrodynamic response analysis has been based on the RAOs, along with a verification by means of the natural frequency for certain DOF. Additionally, the stability of the FHWWP has been assessed. Finally, a discussion on the validity of the methods and results has been presented.

7.1 Case 1: square bow shape

7.1.1 Hydrostatic response

The hydrostatic response has been deducted from the hydrostatic stiffness matrix obtained from the NEMOH simulation, which can be seen in (7.1) below.

$$\mathbf{K}_h = \begin{bmatrix} 0 & 0 & 0 & 0 & 0 & 0 \\ 0 & 0 & 0 & 0 & 0 & 0 \\ 0 & 0 & 4.0221 \times 10^7 & 0 & -9.91 \times 10^2 & 0 \\ 0 & 0 & 0 & 9.5452 \times 10^{10} & 0 & 0 \\ 0 & 0 & -9.91 \times 10^2 & 0 & 2.9890 \times 10^{10} & 0 \\ 0 & 0 & 0 & 0 & 0 & 0 \end{bmatrix} \tag{7.1}$$

By examining the diagonal values in (7.1), it can be concluded that the FHWWP is stable in the motions heave, roll and pitch, due to the fact that the values are positive. If the platform is displaced from the equilibrium position in either one of the three DOF, $\mathbf{K}_h$ indicates that the buoyancy force returns the structure back to the rest position. Consequently, it can be concluded that the FHWWP is statically stable for small angle deviations from the equilibrium position. Besides the diagonal values, the stiffness matrix indicates a coupling between heave and pitch in the off-diagonal values K_{h35}. In essence, the coupling entails that a heave motion can result in a pitch which cannot be restored to the equilibrium position. Contrarily, the coupling indicates that a pitch motion can result in a heave motion which cannot be counteracted by the buoyancy force. However, comparing the magnitude of the off-diagonal values to the diagonals, it can be concluded that the effect of the coupling terms are insignificant.

7.1.2 Hydrodynamic response

The hydrodynamic response of the FHWWP has been obtained by computing the RAOs for all six DOF, which can be seen in Figure 7.1. It is imperative to note that the RAOs shown are only valid for the wave direction of 0°(i.e. in positive x-direction).

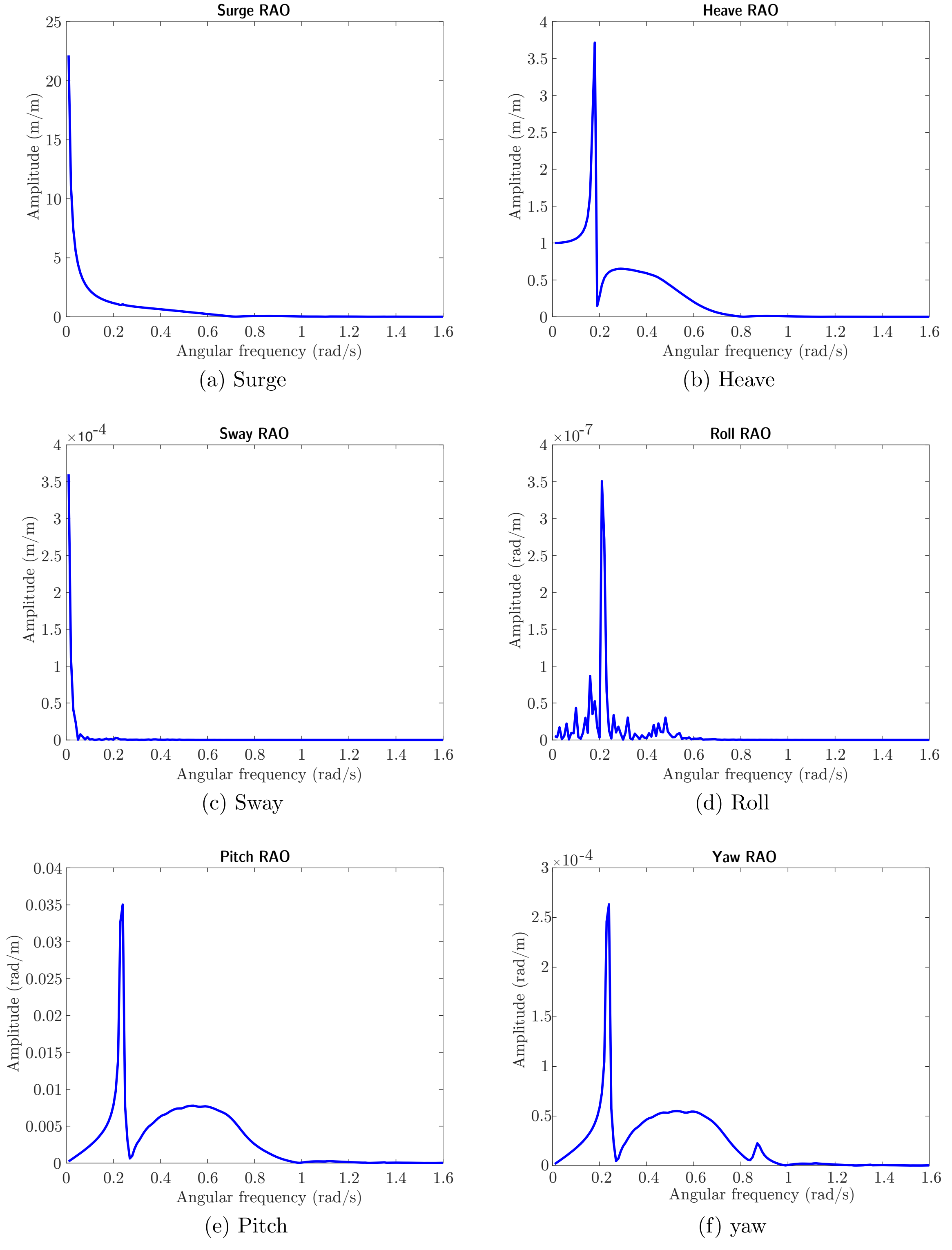

(a) Surge (b) Heave

(c) Sway (d) Roll

(e) Pitch (f) yaw

Figure 7.1: RAOs for the six DOF of the square shape with a wave direction of 0°

Considering the surge behaviour in Figure 7.1a, the exponential shape can be attributed to the fact that the FHWWP has been considered to be a free-floating object, where drag forces on the structure have been neglected. For low frequencies, and therefore for longer wavelengths, the platform experiences significant surge motions as it follows the motion of the waves. However, as the frequency increases, the surge response promptly decreases. Therefore, it can be concluded that waves with higher frequencies and thus shorter wave-lengths have an insignificant interaction with the platform.

As expected, the heave response in Figure 7.1b initiates at an amplitude of 1 m, which coincides with the unitary amplitude of the regular input wave. Therefore, for low frequencies until approximately 0.17 rad/s, the structure follows the wave profile in heave direction. Furthermore, an abrupt peak towards a maximum heave response of 3.7 m can be seen around 0.18 rad/s. The natural frequency in heave at each frequency step has been computed according to (4.15) in subsection 4.2.4. Consequently, in Figure 7.2 below, the natural frequency in heave has been obtained by plotting $\omega_n - \omega$ and finding the zero-crossing. Therefore, it has been verified that the peak occurs at the natural frequency of 0.18 rad/s. It is likely that the abrupt decrease of heave motion after the resonance peak is caused by an anti-resonance frequency. Since the maximum heave response of 3.7 m is significant, it is deemed necessary to consider adding mooring in order to reduce the heave motions. Beyond the resonance frequency, the heave motion significantly decreases to the point where the FHWWP is stationary in heave for higher frequencies.

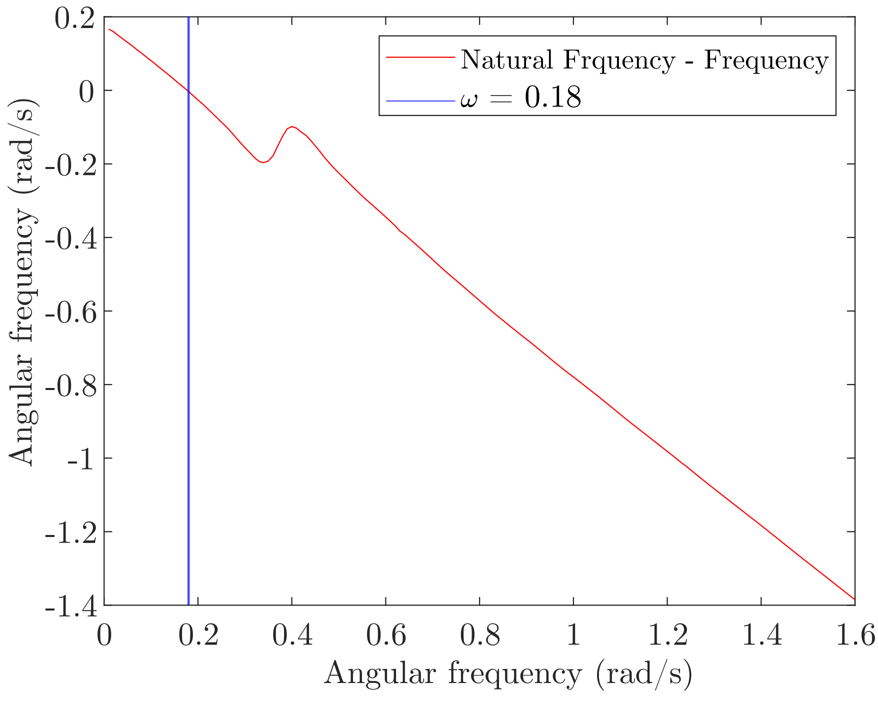

Figure 7.2: Natural frequency in heave

The amplitude response of sway, roll and yaw in Figure 7.1c, 7.1d and 7.1f respectively, is significantly small. Since the input wave direction is in the positive x-direction towards the front of the platform, it is to be expected that the motions in these DOF is limited. Therefore, in the ideal configuration of the FHWWP with the front facing the incident waves, the sway, roll and yaw motions for a regular wave with unitary amplitude have been considered to be negligible.

Finally, the pitch response in Figure 7.1e indicates a maximum pitching motion of $0.035\,\mathrm{rad/m}$, which equals $2°$ in the case of unitary wave amplitude input. Essentially, the RAO indicates that for the given wave input, the FHWWP undergoes a maximum pitching motion from $2°$ to $-2°$ and back. It is evident that this occurs at a resonance frequency of $0.24\,\mathrm{rad/s}$, which has been verified in Figure 7.3 below. Although occurring at the resonance frequency, the maximum pitch angle of $2°$ has been considered to be small. Similar to the other DOF, for higher frequencies, the pitch motion decreases to $0°$.

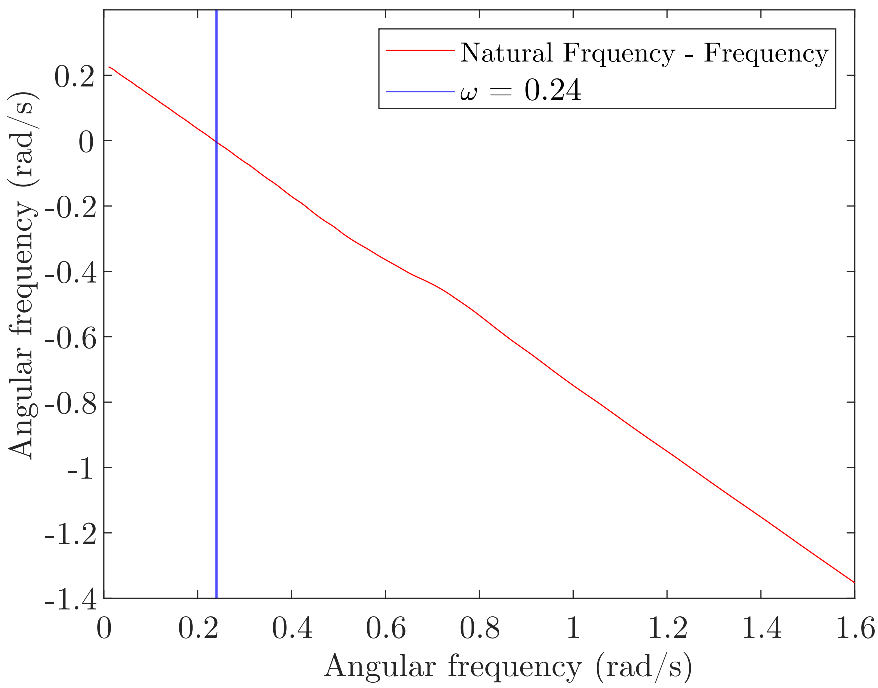

Figure 7.3: Natural frequency in pitch

7.1.3 Stability

Based on the hydrodynamic response for the given wave heading of 0°, the stability is primarily dependent on the motions in surge, heave and pitch since the motions in sway, roll and yaw have been considered to be negligible. Moreover, the lower frequency range of approximately $0.01 < \omega < 1$ is of significant interest in terms of stability as opposed to the higher frequencies $\omega > 1$, since the waves with shorter wave-lengths do not induce motions on the FHWWP, based on the RAOs in Figure 7.1. With regards to the wind-turbine fitted on the platform, the pitching motion is of most significant interest in terms of stability. A transfer function has been fitted to the in- and output frequency data for the pitching motion by means of the SIT, which can be seen in Figure 7.4 below. Consequently, the poles and zeros of the fitted transfer function have been plotted, which can be seen in Figure 7.5. As expected, the system displays oscillatory behaviour with the poles situated at 0 on the real axis. Therefore, the response is not amplified and thus can be deemed stable. In essence, the characteristics of the platform system are stable, which consequently entails that the response is not amplified. In conclusion, it can thus be stated that the FHWWP is stable under the influence of regular waves with unitary amplitude. It is imperative to note that the natural frequency for any motion should be avoided for stability in operational conditions (Aird 2018), or design changes should be implemented such that the natural frequency is not included in a commonly encountered wave frequency range.

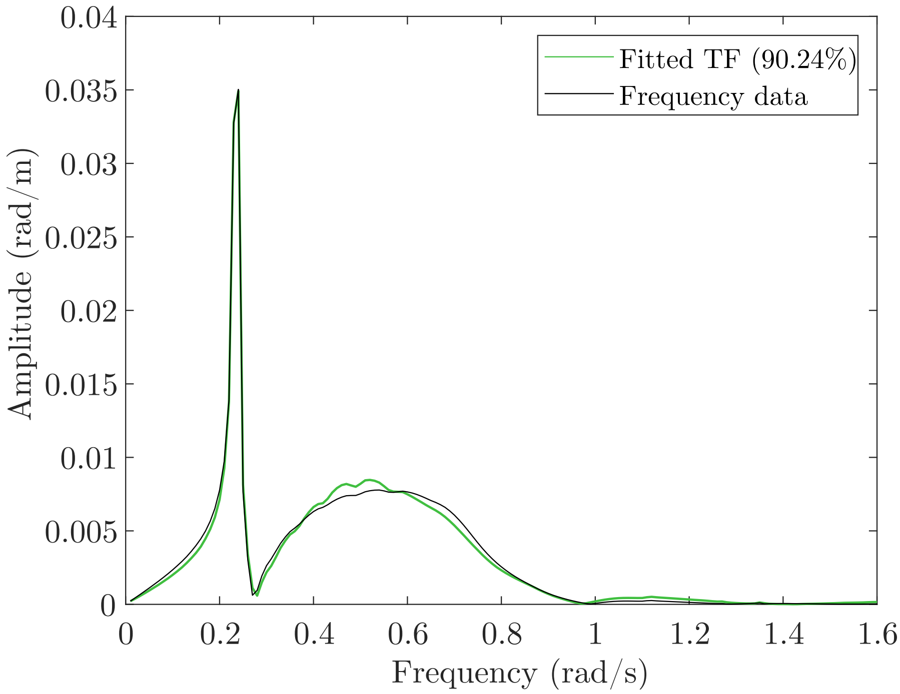

Figure 7.4: Transfer function fitted to pitch frequency data with an accuracy of 90.24%

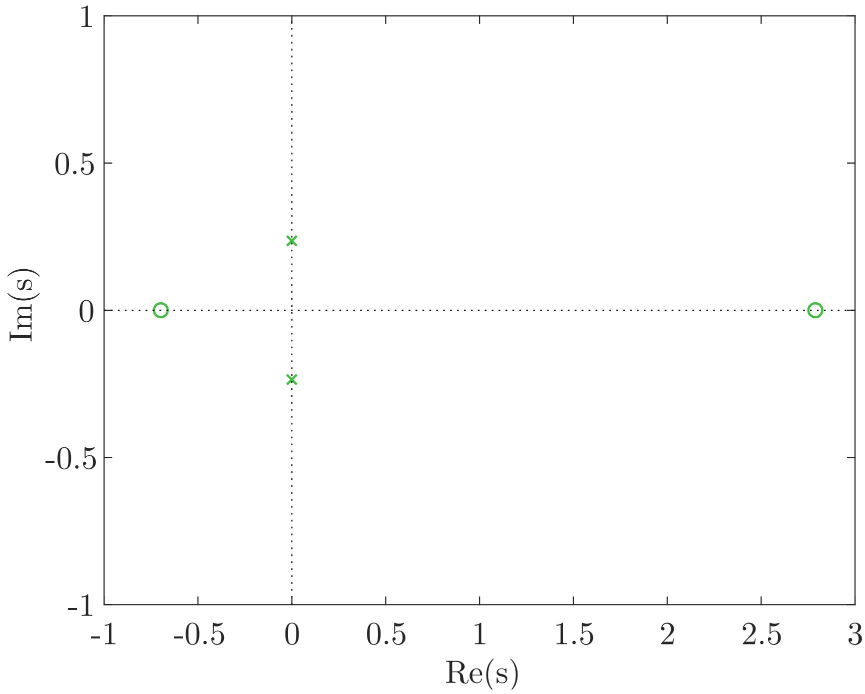

Figure 7.5: Poles (x) and zeros (o) of the fitted transfer function in the complex plane

7.2 Case 2: rounded bow shape

7.2.1 Hydrostatic response

The resulting hydrostatic stiffness matrix for the FHWWP with the rounded bow shape can be seen in (7.2) below.

$$\mathbf{K}_h = \begin{bmatrix} 0 & 0 & 0 & 0 & 0 & 0 \\ 0 & 0 & 0 & 0 & 0 & 0 \\ 0 & 0 & 4.4645 \times 10^{7} & 0 & -14 & \\ 0 & 0 & 0 & 1.0302 \times 10^{11} & 0 & 0 \\ 0 & 0 & -14 & 0 & 4.2845 \times 10^{10} & 0 \\ 0 & 0 & 0 & 0 & 0 & 0 \end{bmatrix} \tag{7.2}$$

In comparison to the stiffness matrix for the square bow platform in (7.1), it can be seen that the coupled off-diagonal terms have decreased and can be considered to be insignificant. Furthermore, the stiffness in the heave and roll motions has slightly increased. Contrarily, the stiffness in pitching motion has increased significantly. The increase can be attributed to the fact that the wetted surface area of the platform has been increased, along with an increase of displaced fluid volume, which consequently have an effect on the buoyancy force. Finally, similar to the square bow structure, the diagonal values in (7.2) have indicated that the rounded structure is statically stable.

7.2.2 Hydrodynamic response

The hydrodynamic response of the platform with rounded bow can be seen in Figure 7.6 below.

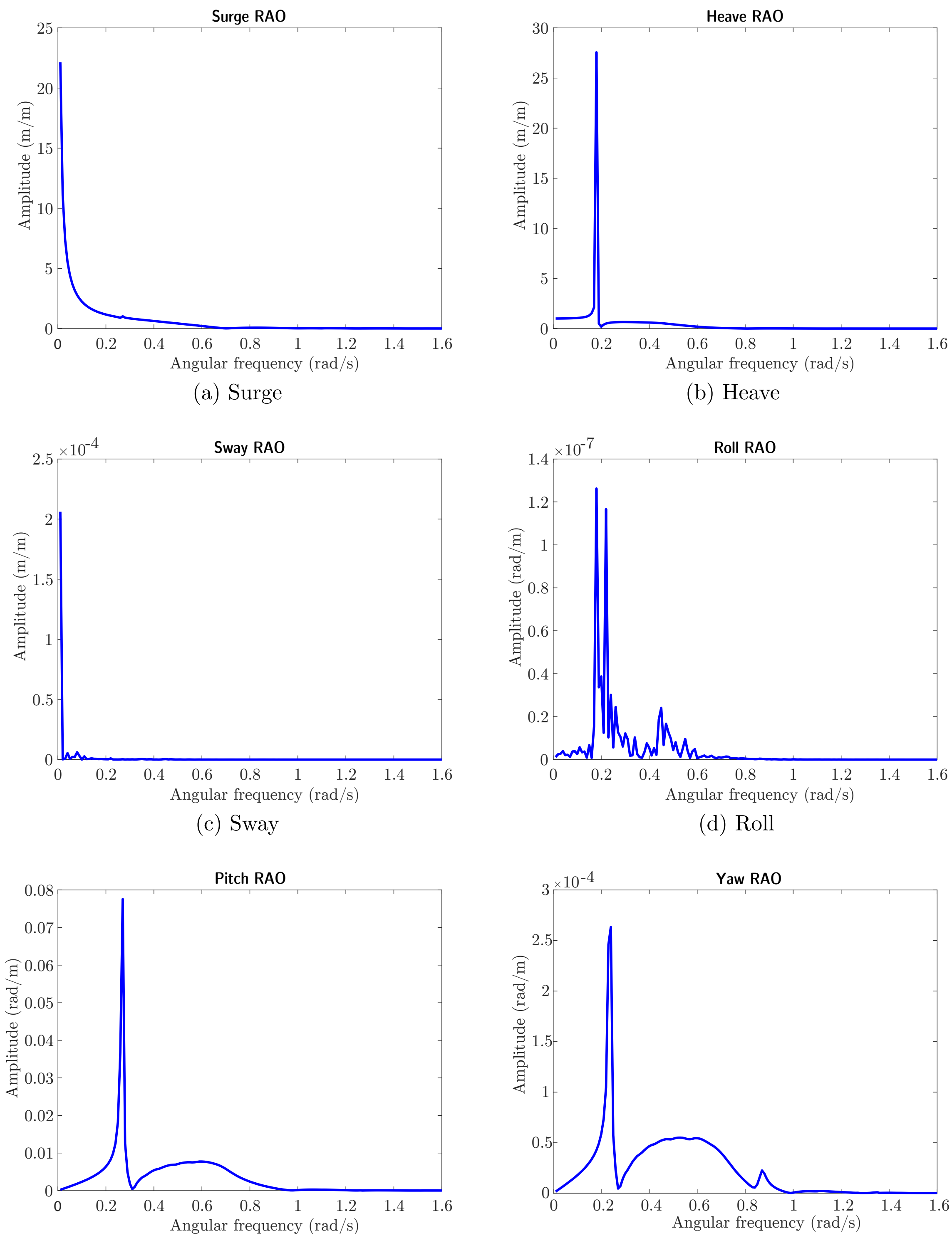

(a) Surge (b) Heave

(c) Sway (d) Roll

(e) Pitch (f) yaw

Figure 7.6: RAOs for the six DOF of the rounded shape with a wave direction of 0°

In comparison to the FHWWP with a square bow shape, the rounded platform shows similar responses in the six DOF. However, the magnitude of the motions differ from the initial simulation.

Surprisingly, the surge behaviour in Figure 7.6a has not been affected by the rounded column shape, where intuitively the surge response should have reduced since the rounded shape allows water to flow through more effortlessly. It is likely that this is due to limitations of NEMOH in accurately considering the quadrangular mesh as a rounded face.

The heave response in Figure 7.6b is similar to the square shape in form as it follows the wave profile for low frequencies and tends to zero after a certain resonance peak. Nonetheless, the maximum heave amplitude of roughly 27 m at the resonance frequency is significantly larger compared to 3.7 m in the first case. It can be considered likely that the significant deviation occurs due to numerical error. In fact, Guo et al. (2017) have indicated that the BEM tends to exaggerate the motion of certain geometries. Moreover, since the free-floating rigid body is essentially modelled as a mechanical oscillator, the increase in maximum heave amplitude could partly be attributed to the increase of overall platform mass due to the addition of the rounded bow faces. Due to the mass increase, the structure reaches a larger maximum heave amplitude at the resonance frequency, which has been determined to be at the same frequency of 0.18 rad/s as for the first case. The derivation of the natural frequency for heave has been presented in Figure 7.7 below.

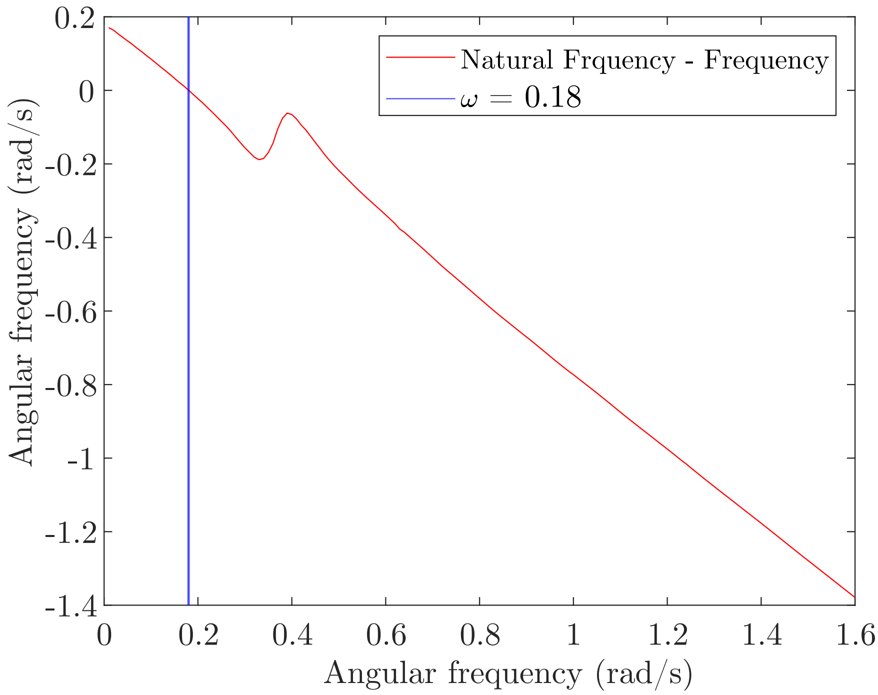

Figure 7.7: Natural frequency in heave for the rounded structure

Comparable to the first case, the responses of the sway, roll and yaw motions in Figure 7.6c, 7.6d and 7.6f are significantly small. In fact, the sway and roll response is noticeably smaller compared to the square bow simulation results.

Finally, similar to the heave response, the maximum pitch amplitude has increased to approximately 0.077 rad/m, or 4.41°. Compared to the first case with a square bow, the maximum pitch amplitude has therefore been doubled. Furthermore, as can be seen in Figure 7.8 below, the resonance frequency for pitch has shifted to 0.27 rad/s, which is a result of the significant increase of hydrostatic stiffness in pitching motion.

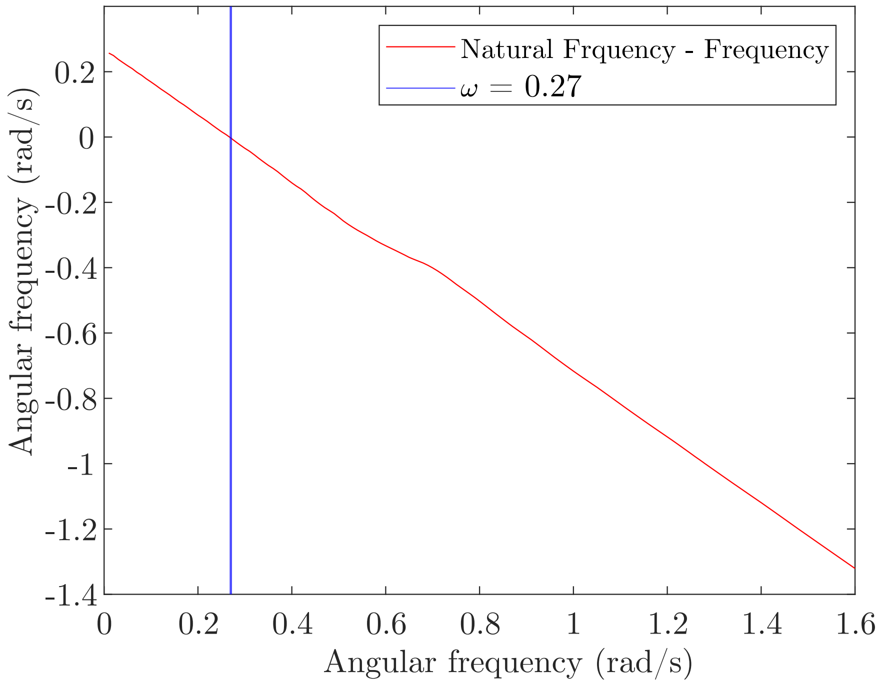

Figure 7.8: Natural frequency in pitch for the rounded structure

7.2.3 Stability

Comparable to the square bow case, the stability is primarily dependent on the motions in surge, heave and pitch. Moreover, the frequency range $0.01 < \omega < 1$ is primarily of interest in terms of stability. Comparable to the first case, a transfer function has been fitted to the frequency data of the pitching DOF, which has been selected due to the significance of the pitching motion to the stability of the structure. The fitted transfer function and the corresponding poles and zeros, as obtained by the SIT can be seen in Figure 7.9 and Figure 7.10 respectively. Similarly to the first case, the location of the poles indicate an oscillating yet stable system characteristics. Therefore, the rounded platform has been deemed stable under the influence of regular waves with unitary wave. Besides, as for the first case, it is imperative to note that the natural frequencies of the respective motions should be avoided or design changes should be implemented such that the natural frequency is not included in a commonly encountered wave frequency range.

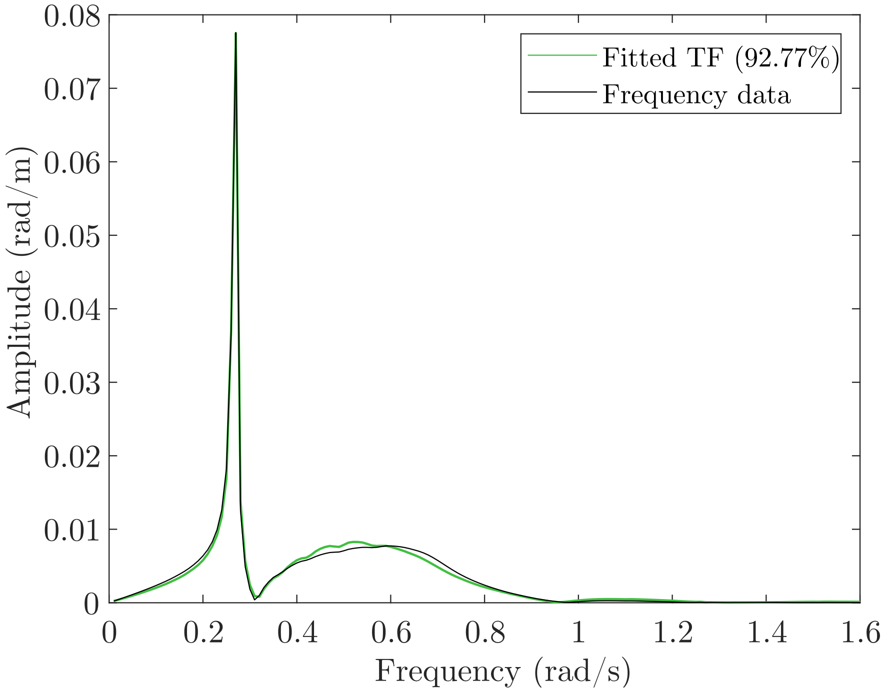

Figure 7.9: Transfer function fitted to pitch frequency data of the rounded structure with an accuracy of 92.77%

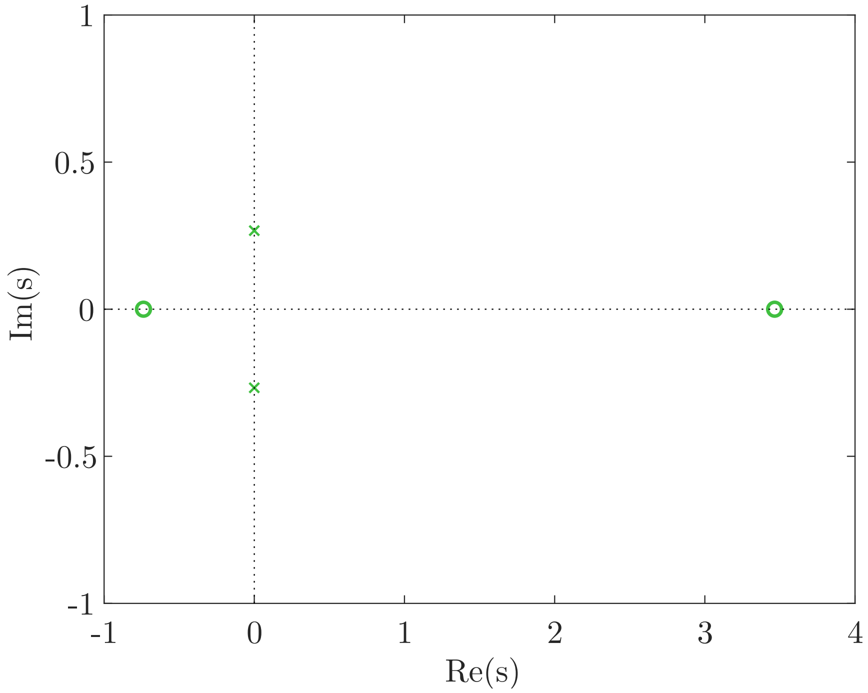

Figure 7.10: Poles (x) and zeros (o) of the fitted transfer function for the rounded structure in the complex plane

7.3 Validation

In any research project, it is significantly important to validate the employed methods and obtained results. As an example, Hall and Goupee (2018) highlight the fact that wave basin testing is an important validation step for floating support structure design. Although the primary focus is on the static and dynamic response and stability analysis, the coefficients obtained from NEMOH should have been validated by wave tank experiments. However, given the completion time of the project of three months, it has not been deemed possible to validate the coefficients using wave basin testing. Nonetheless, the quality of the mesh and the convergence has been assessed in order to ensure a required accuracy from the NEMOH coefficients. Moreover, the correctness of the written RAO MATLAB script has been ensured by firstly considering a more simple and smaller square shape. Finally, the obtained RAOs for the pitch and heave motion have been deemed comparable to the results obtained for a semi-submersible platform of comparable dimensions (Emami et al. 2019). In order to highlight the comparison, the heave RAO has been presented in Figure 7.11 below.

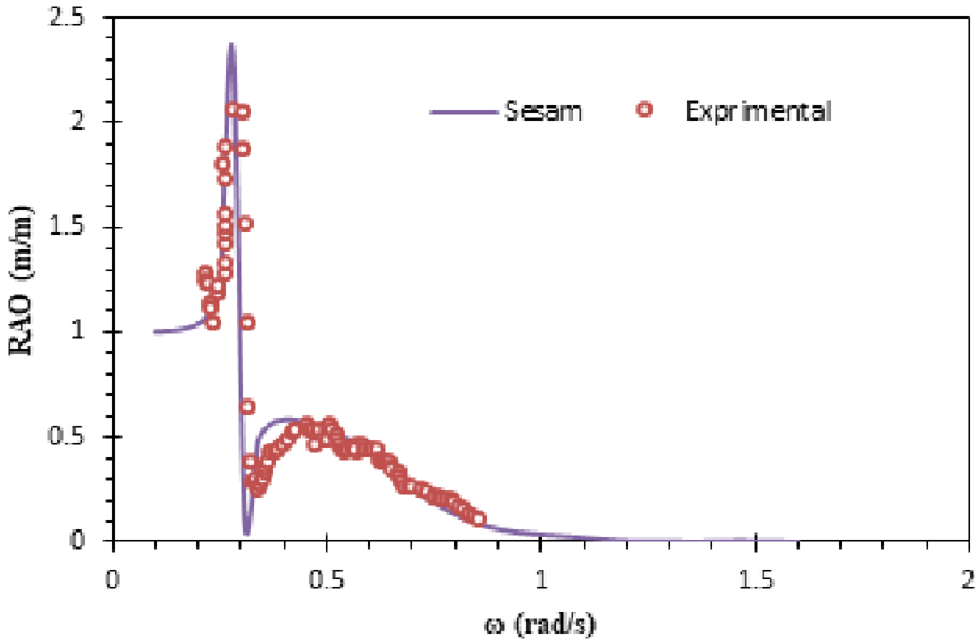

Figure 7.11: Heave RAO for platform with comparable dimensions (Emami et al. 2019)

Although smaller in terms of magnitude, the shape of the response plot appears to be significantly similar to the RAO shown in Figure 7.1b. Although at different frequencies, both plots indicate a certain resonance peak, after which the response decreases to zero at approximately 1 rad/s. In terms of validity, it is imperative to note that the RAO obtained by Emami et al. (ibid.) has been validated with experimental data, as seen in Figure 7.11.

8 Discussion

Due to the fact that several assumptions have been made for a successful completion of the research project, the presented results should be interpreted with a certain caution. The dynamic response of the FHWWP has been determined under the influence of regular waves with unitary amplitude. Although certain sea states might represent such a wave system, it is not suitable for average sea conditions. Moreover, the amplitude of the waves has been assumed to be small in comparison to the wavelength, which entails a small wave steepness. Despite these limiting factors, the response based on the regular wave system has provided a suitable starting point for obtaining the platform motion response. Nonetheless, in order to determine the response to various more realistic sea-states, further research is suggested. Besides the wave input, the BEM has infested certain limitations in terms of linearity. In fact, Guo et al. (2017) have indicated that due to the linearity assumption, BEMs ignore dissipative forces which ultimately results in an exaggeration of motion of certain WEC devices. Therefore, it is possible that the resulted dynamic response of the FHWWP has been exaggerated. Consequently, further research is needed to determine the response more accurately by either applying different methods or extending the BEM to account for non-linearities.

Regarding the FHWWP, the weight of a reference wind-turbine has been incorporated in order to obtain a centre of gravity that accounts for the additional weight. However, the wind-turbine has been approximated as a vertical cylinder of constant diameter. By taking into account the blades, hub and nacelle of the wind-turbine, it is likely that the centre of gravity of the total structure is not situated in the middle, which in turn could significantly affect the dynamic response of the structure. Moreover, the stability assessment does not incorporate the additional moment generated by the wind-turbine hub, nacelle and blades as the structure undergoes a pitching motion.

It has been hypothesised that the rounded bow shape would have a significant impact on the surge response of the floating platform. However, the results have shown that the surge response, in contrast to heave and pitch response, has not been altered. It has been considered likely that this is due to limitations of NEMOH in accurately considering the quadrangular mesh as a rounded face. Therefore, further research is suggested in developing a more suitable or precise mesh in order to determine the surge response of the rounded platform more accurately. Moreover, it could be possible that the analysis on the rounded structure requires a more accurate method than NEMOH for obtaining the RAO.

Finally, it has been decided to only study the influence of waves on the FHWWP. However, it is likely that the wind has a significant effect on the motion and response of the structure. Due to the significant size of the reference wind-turbine, it can be assumed that the wind can generate a significant overturning moment. Therefore, it has been deemed essential to extend the research in order to include the wind interaction, thus obtaining a response that is more true to reality.

9 Conclusion

In conclusion, the respective research questions presented in chapter 3 have been answered and are revisited in this chapter. Firstly, the equation of motion has been developed in chapter 4, which describes the motion of a free floating platform under the influence of regular waves. Although simplified by assuming linearity and linear potential theory, a sufficient equation of motion has been obtained in the frequency domain, in order to directly utilise the results from NEMOH. The obtained equation of motion has formed the basis for the RAO calculations.

Secondly, the design characteristics of the FHWWP have been collected from the problem owner and thereafter utilised in an embodiment which has been constructed in Solidworks. Consequently, the embodiment has been used in order to determine the centre of gravity of the full structure, including a reference 8 MW wind-turbine. Moreover, the embodiment has been meshed in COMSOL in order to implement the embodiment into the NEMOH analysis. Besides the basic platform shape, a COMSOL mesh with a rounded bow shape has been created in order to verify the effect on surge motion.

Thirdly, the hydrostatic response of the FHWWP has been obtained from the NEMOH analysis after implementing the COMSOL meshes and characteristics such as centre of gravity and frequency range. The resulting hydrostatic matrices have indicated that both the square and round shaped platforms can be considered to be statically stable. Essentially, it has been shown that for small angle excitations, both platforms return to the upright equilibrium position due to the shifted buoyancy force, based on the diagonal values obtained in the hydrostatic stiffness matrix.

Fourthly, the hydrodynamic response for all DOF in the frequency domain for both platform shapes has been obtained from the NEMOH data. The obtained RAO plots have indicated the motion response in each DOF. As expected with the given wave direction of $0°$, motions in roll, sway and yaw have not been recorded. The maximum heave motion of the square and rounded platform have been defined to be 3.7 m and 27 m respectively. The maximum pitch of the square and rounded platform has been evaluated at $2°$ and $4.41°$ respectively. Regarding the surge motion, both platforms exhibit significantly large motions for low wave frequencies. In contrast to what has been hypothesised, the surge motion has not been reduced by the introduction of a rounded bow shape. Moreover, the natural frequency of heave and pitch motion has been obtained, which coincides with the peaks in the respective RAO graphs.

Finally, the stability of the FHWWP with both bow shapes has been assessed by means of fitting a transfer function to the frequency pitch data obtained from NEMOH for the hydrodynamic response analysis. Based on the location of the poles of both transfer functions, it has been concluded that the system characteristics are stable. Therefore, the response is not amplified by the system. Additionally, it has been concluded that the previously specified natural frequencies should continually be avoided in order to maintain stability of the floating structure.

Bibliography

Aird, Peter (2018). *Deepwater Drilling: Well Planning, Design, Engineering, Operations, and Technology Application*. Gulf Professional Publishing.

Ansys, AQWA (2014). “Theory manual”. In: *ANSYS, Editor, ANSYS® Academic Research*.

Armaroli, Nicola and Vincenzo Balzani (2016). “Solar electricity and solar fuels: status and perspectives in the context of the energy transition”. In: *Chemistry–A European Journal* 22.1, pp. 32–57.

Babarit, A and G Delhommeau (2015). “Theoretical and numerical aspects of the open source BEM solver NEMOH”. In: *In Proc. of the 11th European Wave and Tidal Energy Conference (EWTEC2015)*.

Borouchaki, Houman, Patrick Laug, and Paul-Louis George (2000). “Parametric surface meshing using a combined advancing-front generalized Delaunay approach”. In: *International Journal for Numerical Methods in Engineering* 49.1-2, pp. 233–259.

Collu, Maurizio et al. (2014). “Stability requirements for floating offshore wind turbine (FOWT) during assembly and temporary phases: Overview and application”. In: *Ocean engineering* 84, pp. 164–175.

Desmond, Cian et al. (2016). “Description of an 8 MW reference wind turbine”. In: *Journal of Physics: Conference Series*. Vol. 753. 9. IOP Publishing, p. 092013.

Emami, Arefeh et al. (2019). “Pitch Motion Response of an Equipped Semi-Submersible Platform with Tuned Sloshing Dampers”. In: *International Journal of Coastal and Offshore Engineering* 3.1, pp. 47–54.

Failla, Giuseppe and Felice Arena (2015). *New perspectives in offshore wind energy*.

Falnes, Johannes and Adi Kurniawan (2020). *Ocean waves and oscillating systems: linear interactions including wave-energy extraction*. Vol. 8. Cambridge university press.

Faltinsen, Odd (1993). *Sea loads on ships and offshore structures*. Vol. 1. Cambridge university press.

FAS (2008). *Principles of stability*. URL: `https://fas.org/man/dod-101/navy/docs/swos/dca/stg4-01.html` (visited on 04/15/2020).

Gielen, Dolf et al. (2019). “The role of renewable energy in the global energy transformation”. In: *Energy Strategy Reviews* 24, pp. 38–50.

Guo, Bingyong et al. (2017). “Nonlinear modeling and verification of a heaving point absorber for wave energy conversion”. In: *IEEE transactions on sustainable energy* 9.1, pp. 453–461.

Hall, Matthew and Andrew J Goupee (2018). “Validation of a hybrid modeling approach to floating wind turbine basin testing”. In: *Wind Energy* 21.6, pp. 391–408.

IRENA (2019). *Global energy transformation: A roadmap to 2050*.

Jurado, Antonio Manuel Pegalajar, Michael Borg, and Henrik Bredmose (2018). “An efficient frequency-domain model for quick load analysis of floating offshore wind turbines”. In: *Wind Energy Science* 3.2, pp. 693–712.

Konovessis, Dimitris, Kie Hian Chua, and Dracos Vassalos (Dec. 2013). "Stability of floating offshore structures". In: *Ships and Offshore Structures* 9, pp. 125–133. DOI: 10.1080/17445302.2012.747270.

Liu, Yichao et al. (2016). "Developments in semi-submersible floating foundations supporting wind turbines: A comprehensive review". In: *Renewable and Sustainable Energy Reviews* 60, pp. 433–449.

Massie, WW and JM Journée (2001). "Offshore hydromechanics". In: *Delft University of Technology: Delft, The Netherlands*.

MIT (2020). *Understanding Poles and Zeros*. URL: http://web.mit.edu/2.14/www/Handouts/PoleZero.pdf (visited on 06/03/2020).

Molland, Anthony F (2011). *The maritime engineering reference book: a guide to ship design, construction and operation*. Elsevier.

Muetze, Annette and JG Vining (2006). "Ocean wave energy conversion-a survey". In: *Conference record of the 2006 IEEE industry applications conference forty-first IAS annual meeting*. Vol. 3. IEEE, pp. 1410–1417.

Newman, John Nicholas (2018). *Marine hydrodynamics*. MIT press.

Nolte, Jerica D and RC Ertekin (2014). "Wave power calculations for a wave energy conversion device connected to a drogue". In: *Journal of Renewable and Sustainable energy* 6.1, p. 013117.

Paramor, OAL et al. (2009). *MEFEPO North Sea Atlas*. University of Liverpool.

Payne, Gregory S et al. (2008). "Assessment of boundary-element method for modelling a free-floating sloped wave energy device. Part 1: Numerical modelling". In: *Ocean Engineering* 35.3-4, pp. 333–341.

Pérez-Collazo, Carlos, D Greaves, and G Iglesias (2015). "A review of combined wave and offshore wind energy". In: *Renewable and Sustainable Energy Reviews* 42, pp. 141–153.

Thiagarajan, KP and HJ Dagher (2014). "A review of floating platform concepts for offshore wind energy generation". In: *Journal of offshore mechanics and Arctic engineering* 136.2.

Vantorre, Marc, Robert Banasiak, and Ronny Verhoeven (2004). "Modelling of hydraulic performance and wave energy extraction by a point absorber in heave". In: *Applied Ocean Research* 26.1-2, pp. 61–72.

Wei, Y et al. (2019). "Frequency-domain hydrodynamic modelling of dense and sparse arrays of wave energy converters". In: *Renewable energy* 135, pp. 775–788.

Yang, Wenxian et al. (2019). "Experimental research for stabilizing offshore floating wind turbines". In: *Energies* 12.10, p. 1947.

Zhang, D and EG Paterson (2015). "A study of wave forces on an offshore platform by direct CFD and Morison equation". In: *E3S Web of Conferences*. Vol. 5. EDP Sciences, p. 04002.

A MATLAB scripts

A.1 NEMOH

```
%Author: Jorrit Sijtsma
%Script that first describes the parameters of the geometry,
    then initiates the Nemoh mesh code.

load('Comsol2Nemoh_800_v2.mat');
%platform is only 1 body.
nBodies=1;

%number of quadrangular panels
n=size(X,2);

%center of gravity, obtained from platform embodiment.
CG(1,:)=[0. 0. -16.94];

%no translations needed due to origin location / symmetry in
    xOz
tX(1)=0;

%target number of panels.
nfobj(1)=800;

%call Nemoh meshing function.
[Mass,Inertia,KH,XB,YB,ZB]=Mesh(nBodies,n,X,tX,CG,nfobj);

%save parameters needed in further analysis
save('hydrostat_comsol_800_v2', 'KH', 'Mass', 'Inertia', 'XB'
    , 'YB', 'ZB')
```

Listing A.1: Nemoh mesh script

```
%Author: Jorrit Sijtsma
%Script to initiate and run the Nemoh code for obtaining the
   hydrodynamic coefficients

% Vector of wave frequencies (rad/s)
w = [0.01:0.01:1.6];

%wave direction in degrees, 0 in positive x direction
dir = 0 ;

%water depth (m), 0 for deep water.
depth = 200 ;

[A,B,Fe]=Nemoh(w, dir, depth);

%save function for outputs
save('hydrodyn_comsol_800_v2', 'A','B','w','Fe')
```

Listing A.2: Nemoh solver script

A.2 RAO calculations and post-processing

```
%Author: Jorrit Sijtsma
%Script to compute the RAO for 6DOF, using the data obtained
   from NEMOH.

clear all;
clc;
%Coordinate system: (xyz)

load('hydrostat_comsol_800_v2.mat');
load('hydrodyn_comsol_800_v2.mat');

%Preallocating / preparing several parameters
z=zeros(6,length(w));
omega=zeros(length(w):1);
Fet=transpose(Fe);
M=zeros(6,6);
Kh=zeros(6,6);

%Specify the DOF to plot
dof=5;

%Wave input amplitude is 1 by default from NEMOH
amplitude=1;

```

```
%transforming 1x6x6 inertia matrix to 6x6 mass matrix (M) and
    1x6x6 KH matrix to 6x6 Kh stiffness matrix
for n=1:6
    M(n,:)=Inertia(:,:,n);
    Kh(n,:)=KH(:,:,n);
end

%solving for each frequency as specified by the vector w
for j=1:length(w)
omega=w(1,j);
omega2=omega*omega;

Term1= -omega2*(M+A(:,:,j));

Term2= 1i*omega*B(:,:,j);

Term3= Kh;

H=Term1 + Term2 + Term3;
Htransfer=inv(H.*amplitude);

%calculation of displacement vector in frequency domain
z(:,j)=Htransfer*Fet(:,j);

end

%extracting modulus of complex frequency signal for amplitude
Rao=abs(z);

figure(1);
Raoplot=Rao(dof,:);
plot(w,Raoplot,'-b','LineWidth',2);
title('Pitch RAO');
xlabel('Angular frequency (rad/s)');
ylabel('Amplitude (rad/m)');

%extracting the phase of the RAO signal
Raophase=angle(z);

figure(2);
plot(w,Raophase(dof,:),'-*r');
title('RAO pitch phase');
```

Listing A.3: RAO calculation script

A.3 Natural frequency

```
%Author: Jorrit Sijtsma
%Natural frequency
%omegan=sqrt(KH/(M+A))=omega

load('hydrostat_comsol_800_v2');
load('hydrodyn_comsol_800_v2');
omegan=zeros(1,length(w));

%specify motion (5=pitch)
dof=5;

for n=1:6
    M(n,:)=Inertia(:,:,n);
    Kh(n,:)=KH(:,:,n);
end

for j=1:length(w)
    Term1=Kh(dof,dof)/(M(dof,dof)+A(dof,dof,j));

    omegan(:,j)=sqrt(Term1);

end

%substract w to find wn at 0.
omegaplot=omegan-w;

plot(w,omegaplot,'-r');
hold on;
xline(0.24,'b');
xlabel('Angular frequency (rad/s)')
ylabel('Angular frequency (rad/s)')
legend('Natural Frquency - Frequency','\omega = 0.24')
```

Listing A.4: Natural frequency calculation script

B System Identification Toolbox

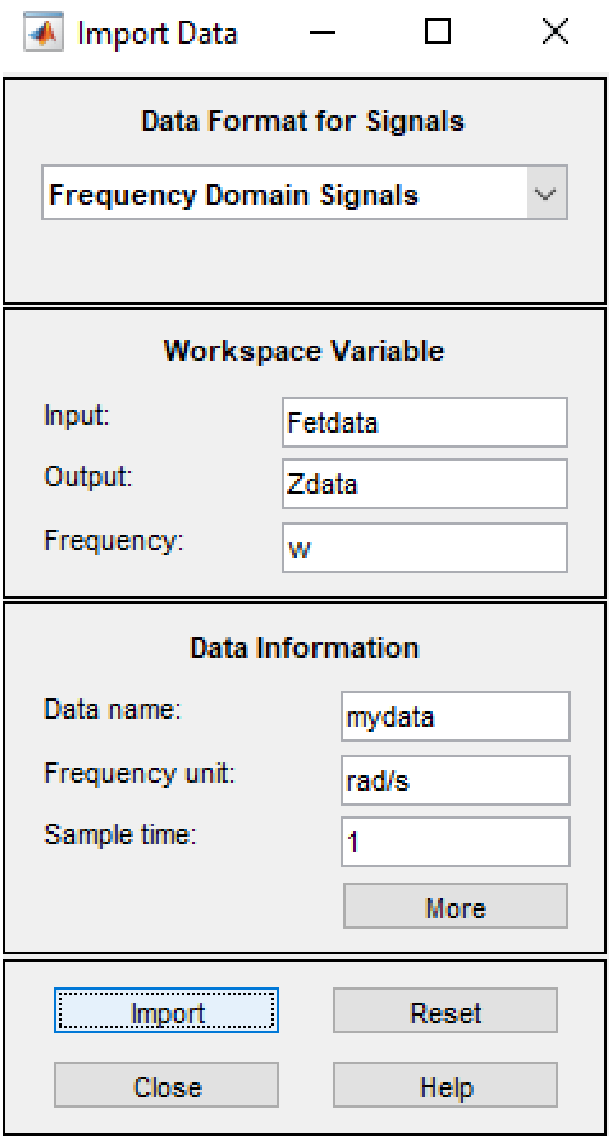

Figure B.1: Data import panel SIT

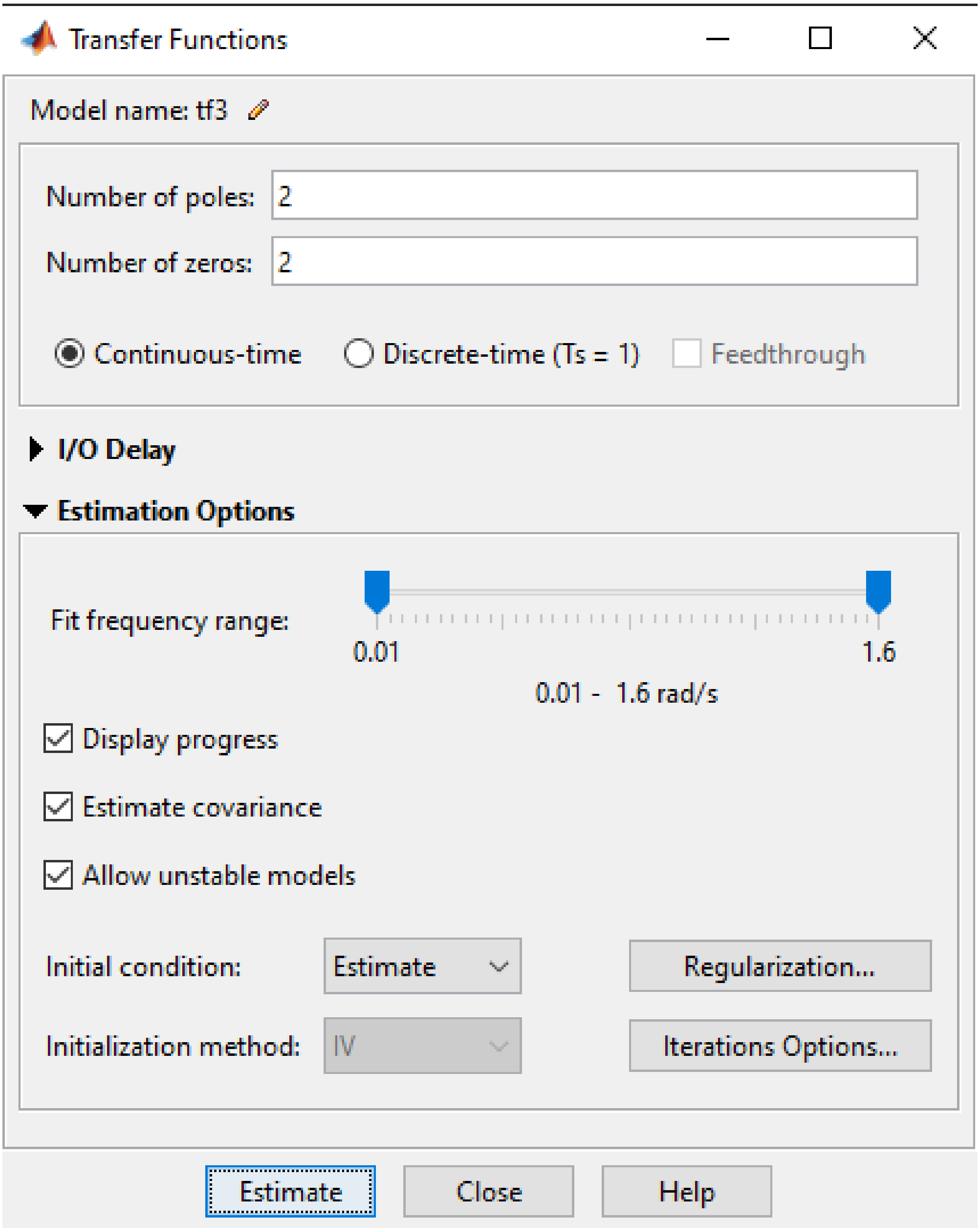

Figure B.2: Transfer function estimation panel SIT

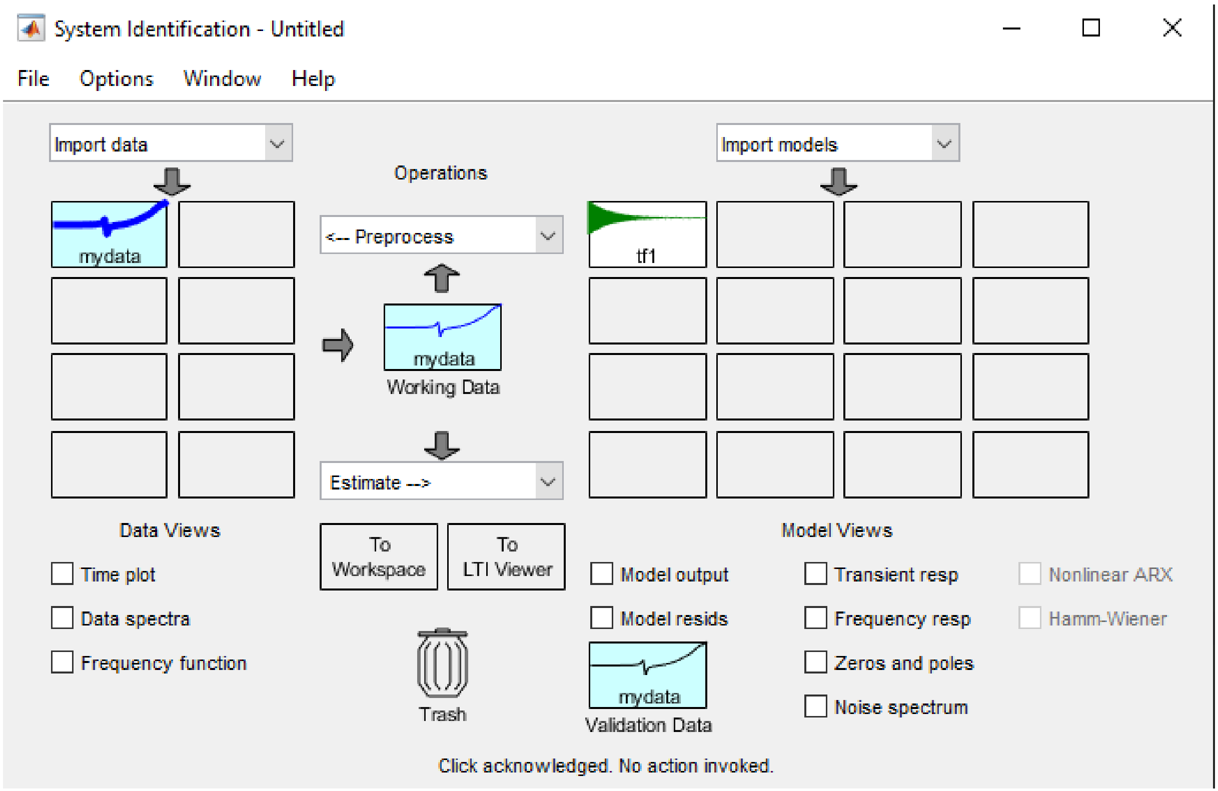

Figure B.3: SIT dashboard panel